Title

Capturing Spatial Variability of Biogeochemical Mass Exchanges and Reaction Rates in Wetland Water and Soil through Model Compartmentalization

Journal

Journal of Hydrologic Engineering, 22(1)

ISSN

1084-0699

Authors

Sharifi, A
Kalin, L
Asce, AM
et al.

Publication Date

2017

DOI

10.1061/(asce)he.1943-5584.0001196

Peer reviewed

Capturing Spatial Variability of Biogeochemical Mass Exchanges and Reaction Rates in Wetland Water and Soil through Model Compartmentalization

A. Sharifi[1]; L. Kalin, A.M.ASCE[2]; M. M. Hantush, A.M.ASCE[3]; R. A. Dahlgren[4]; A. T. O'Geen[5]; and J. J. Maynard[6]

Abstract: A common phenomenon observed in natural and constructed wetlands is short-circuiting of flow and formation of stagnant zones that are only indirectly connected with the incoming water. Biogeochemistry of passive areas is potentially much different than that of active zones. In the research reported in this paper, the spatial resolution of a previously developed wetland nutrient cycling model was improved in order to capture the spatial variability of concentrations and reaction rates regarding nitrogen and carbon cycles throughout active and passive zones of wetlands. The upgraded model allows for several compartments in the horizontal domain, with all neighboring compartments connected through advective and dispersive/diffusive mass transport. The model was applied to data collected from a restored wetland in California that was characterized by the formation of a large stagnant zone at the southern end of the wetland due to close vicinity of the inlet and outlet structures in the northern end. Mass balance analysis revealed that over the course of the research period, about 23.4 $\pm$ 3.9% of the incoming total nitrogen load was removed or retained by the wetland. It was observed that mass of all exchanges (physical and biogeochemical) regarding nitrogen cycling decreased along the activity gradient from active to passive zones. Model results also revealed that anaerobic processes become more significant along the activity gradient towards passive areas. **DOI: 10.1061/(ASCE)HE.1943-5584.0001196.**

Introduction

Wetlands have been widely recognized as effective means for water quality improvement and alleviation of nonpoint-source pollution associated with agricultural runoff (Mitsch and Gosselink 2007). A common phenomenon that is observed in natural and constructed wetlands is short-circuiting of flow and formation of stagnant zones that are only indirectly available to the inflow waters (Min and Wise 2009). Such stagnant zones can offset treatment effectiveness of wetlands by reducing active volume and consequently shortening the hydraulic retention time (Kadlec and Wallace 2008). Many natural and constructed wetlands are characterized by a deeper open channel in the middle and shallower stagnant zones with emergent vegetation on the periphery. Soil characteristics, plant composition, and physical and biogeochemical processes of the main channel can be potentially contrasting to those of stagnant zones on the periphery. The main channel conveys a large amount of flow, thus not supporting emergent macrophytes, whereas the stagnant zones are ideal for emergent vegetation. A study by Anderson et al. (2006) on two constructed wetlands detected higher mean sediment accumulation in the deeper open water zones than in the emergent vegetation zones. In contrast, researchers reported higher organic carbon concentrations in the sediment of stagnant zones. Another finding of Anderson et al. (2006) was a gradual decrease in accumulation of sediment from inflow to outflow in deeper water zones.

Wetland models are useful tools for understanding complex interactions between wetland soil, hydrology and vegetation. Biogeochemistry of passive areas is potentially different than that of active zones (Reddy and Delaune 2008), making it difficult for lumped wetland models to capture the dynamics of biogeochemical exchanges within (and between) active and passive areas of the wetland. When there is nonuniformity in water flow and geochemical reactions throughout the wetland, a more sophisticated wetland model is needed to overcome the limitations of lumped models. One practical method of increasing model proficiency for demonstrating nonuniform wetlands is through compartmentalization of the model. In such a method, the underlying differential equations are discretized numerically, such that instead of having one lumped model representing the whole wetland environment, there will be several compartments dedicated to distinct hydrologic and biogeochemical zones within the wetland environment. A compartmentalized model allows a better comprehension of hydrologic and biogeochemical processes within active and passive areas, as well as a chance of achieving better model performance in validation. Through sensitivity analysis, a distributed model can reveal the sensitivity of various compartments (each representing a specific biogeochemical zone) to different processes, thus revealing the importance of such processes in various areas within the wetland.

[1]Research Associate, Univ. of Maryland, 10300 Baltimore Ave., Bldg. 007, Barc-West, Beltsville, MD 20705 (corresponding author). E-mail: amirrezasharifi@gmail.com

[2]Associate Professor, Auburn Univ., 602 Duncan Dr., Auburn, AL 36849.

[3]Research Hydrologist, National Risk Management Research Laboratory, U.S. EPA, 26 West Martin Luther King Dr., Cincinnati, OH 45268.

[4]Professor, Univ. of California, One Shields Ave., Davis, CA 95616-8627.

[5]Soil Resource Specialist in Cooperative Extension, Univ. of California, One Shields Ave., Davis, CA 95616-8627; Professor, Univ. of California, One Shields Ave., Davis, CA 95616-8627.

[6]Postdoctoral Research Ecologist, Jornada Experimental Range, Agricultural Research Service (ARS), USDA, P.O. Box 30003, MSC 3JER, New Mexico State Univ., Las Cruces, NM 88003.

Note. This manuscript was submitted on September 26, 2014; approved on January 29, 2015; published online on March 18, 2015. Discussion period open until August 18, 2015; separate discussions must be submitted for individual papers. This paper is part of the ***Journal of Hydrologic Engineering***, © ASCE, ISSN 1084-0699/D4015001(18)/$25.00.

In the research reported in this paper, the spatial resolution of a previously developed wetland nutrient cycling model, namely the *WetQual* model (Sharifi et al. 2013; Hantush et al. 2013), was improved in order to capture the spatial variability of concentrations and reaction rates regarding nitrogen, phosphorus, and carbon cycles throughout active and passive zones of wetlands. A previous version of the *WetQual* model was comprised of three compartments in the vertical domain (z), including (1) standing water, (2) aerobic soil, and (3) anaerobic soil, and lumped in the horizontal domain (xy–plane), thus qualifying *WetQual* as a quasi-one-dimensional (1D) model. In the research reported in this paper, the model was enhanced to a quasi-three-dimensional (3D) state by discretizing the horizontal domain (lateral and longitudinal) into compartments, and connecting neighboring compartments through advective and dispersive/diffusive exchange. In general terms, a compartment is defined as a volume of medium within which the chemical concentrations do not vary spatially and thus system parameters are constant (Little 2012). The spatial domain of the wetland is abstracted as a set of compartments, with the total number of compartments reflecting the desired spatial resolution.

The compartmental model was applied to data collected from a restored wetland receiving agricultural runoff on the west side of the San Joaquin River in California's Central Valley during the 2007 growing season (May–September; Maynard 2009; Maynard et al. 2011). Due to close vicinity of inflow and outflow structures in the northern end, a large stagnant zone was created in the southern portion of the wetland, which constitutes more than 50% of the wetland area (Maynard 2009). Through detailed sensitivity and mass balance analyses, the most important processes engaging nitrogen and carbon constituents along the activity gradient line (i.e., active to passive transition zone) were investigated.

Computer Model

WetQual is a process-based model for sediment, nitrogen, phosphorus, and carbon retention, cycling, and removal in flooded wetlands (Hantush et al. 2013; Kalin et al. 2013; Sharifi et al. 2013). The model simulates oxygen dynamics and the impact of oxidizing and reducing conditions on nitrogen and carbon transformation and removal, as well as phosphorus retention and release. *WetQual* explicitly accounts for nitrogen loss pathways of volatilization and denitrification and considers various biogeochemical interactions affecting carbon cycling, methane emissions, and organic carbon export and retention. The model separates free-floating plant biomass (e.g., phytoplankton) from rooted aquatic plants and uses a simple model for plant productivity in which the daily growth rate is related to daily solar radiation and annual growth rates of plants. In the vertical domain, *WetQual* partitions a wetland into three basic compartments consisting of the water column (free water) and two wetland soil layers. The vertical soil layer is partitioned into aerobic and anaerobic zones where the boundary between the two zones fluctuates up or down based on competing oxygen supply and removal rates. Readers are referred to Hantush et al. (2013), Kalin et al. (2013), and Sharifi et al. (2013) for more detailed information regarding model structure, governing equations, and case study applications of *WetQual*.

Compartmentalization Approach

In the *WetQual* model, for each constituent, a set of three ordinary differential equations (ODEs) was coupled to explain the variation of concentration in the water and sediment columns. It was assumed that concentrations were spatially uniform throughout the whole wetland in the horizontal domain, i.e., xy–domain.

For a generic dissolved constituent in the water column, the ordinary differential equation representing mass balance was given by

$$\phi_w \frac{dV_w C_w}{dt} = Q_{\text{in}} C_{\text{in}} - Q_{\text{out}} C_w - k\phi_w V_w C_w + \beta_1 A(C_s - C_w) + F^w_{C_{Dg}} \tag{1a}$$

$$F^w_{C_{Dg}} = \begin{matrix} Q_g C_s, Q_g > 0 \\ Q_g C_w, Q_g < 0 \end{matrix} \tag{1b}$$

The left-hand side of Eq. (1*a*) explains variation of concentration (C_w) over time in the water column [C_w is concentration of dissolved constituents in free water (ML^{-3}), ϕ_w is effective porosity of wetland surface water, and V_w is the volume of wetland surface water (L^3)] and the four terms on the right-hand-side, respectively, explain (1) direct loading gain through inflow, (2) loss through outflow, (3) loss through internal decay, and (4) exchanges between water and sediment columns through diffusive transport and infiltration/groundwater exchange [Q_{in} is volumetric inflow rate ($\text{L}^3\ \text{T}^{-1}$), C_{in} is constituent concentrations in incoming water (ML^{-3}), Q_{out} is wetland discharge (outflow) rate ($\text{L}^3\ \text{T}^{-1}$), $F^w_{C_{Dg}}$ is groundwater exchange/infiltration loss, Q_g is groundwater flow ($\text{L}^3\ \text{T}^{-1}$) that can be either positive [upwards, discharging to the wetland] or negative (downwards, net infiltration recharging groundwater table), k is collective rate of mass losses to aerobic and anaerobic respiration (T^{-1}), β_1 is the diffusive mass-transfer rate of dissolved constituent between wetland water and aerobic soil layer (LT^{-1}), A is wetland surface area (L^2), and C_s is the pore water constituent concentrations in aerobic sediment layer (ML^{-3})].

In the compartmental approach, the wetland was further divided into compartments or volumes in the horizontal domain, and a set of three coupled differential equations was established for each compartment. Concentrations and parameters (coefficients) were assumed to be spatially uniform within each compartment (as opposed to the whole wetland). Fig. 1 shows a two-dimensional (2D) schematic of a hypothetical compartmentalized wetland. Under this compartmental modeling approach, Eqs. (1*a*) and (1*b*) were rewritten for each compartment as

$$\phi_{w.i} \frac{dV_i C_{w.i}}{dt} = Q_{\text{in}.i} C_{\text{in}.i} - Q_{\text{out}.i} C_{w.i} + \sum_{j=1,n_i} (Q_{j,i} C_{w.j} - Q_{i,j} C_{w.i}) + \sum_{j=1,n_i} \beta_{i,j} A_{i,j} (C_{w.j} - C_{w.i}) - k_i \phi_{w.i} V_{w.i} C_{w.i} + \beta_1 A_i (C_{s.i} - C_{w.i}) + F^w_{C_{Dg}} \tag{2a}$$

$$F^w_{C_{Dg}} = \begin{matrix} Q_{g.i} C_{s.i}, Q_{g.i} > 0 \\ Q_{g.i} C_{w.i}, Q_{g.i} < 0 \end{matrix} \tag{2b}$$

where i = index for compartment i, thus $C_{w.i}$ becomes the average constituent concentration of compartment i and $V_{w.i}$ is the volume of compartment i, and so on. There are two additional terms that appear in Eq. (2*a*), i.e., the third and fourth terms on the right-hand side, which explain the advective and diffusive/dispersive mass exchanges between the compartments. The term $Q_{i,j}$ is the advective flow rate across the interface from compartment i to j($\text{L}^3\ \text{T}^{-1}$); $\beta_{i,j}$ is the dispersive/diffusive mass transfer rate (LT^{-1}) across boundary i, j, $A_{i,j}$ is the area (L^2) of the interface between compartments i and j, and n_i is the number of compartments surrounding compartment i.

Advective Exchange

As shown in Fig. 1, the new compartmental scheme allows for external inflows and outflows to/from any adjacent compartment within the wetland. Accurate estimation of advective flow rates

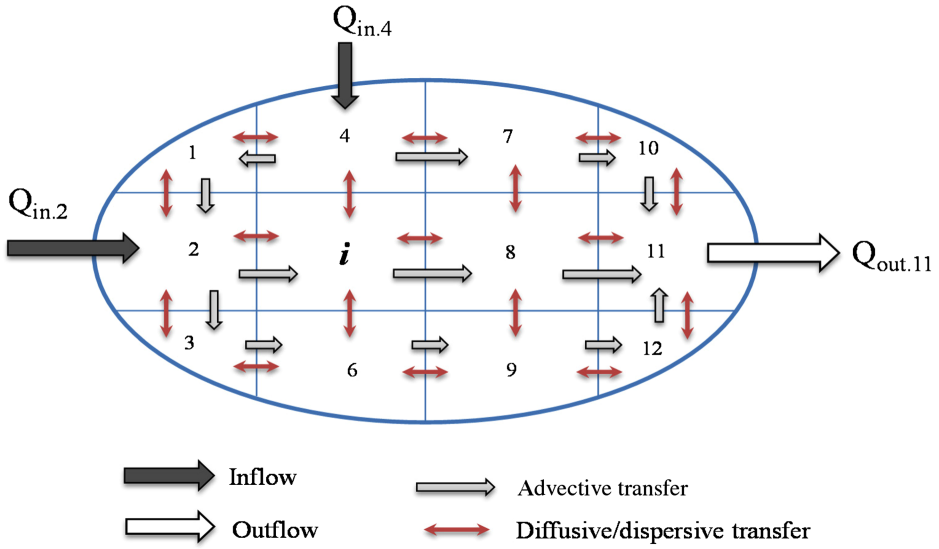

Fig. 1. Schematic plan of a compartmentalized wetland

across the interface between compartments [$Q_{i,j}$ in Eqs. (2*a*) and (2*b*)] is critical. Where the geometry of the study wetland is simple (e.g., single inlet and outlet wetland, compartments in series), a flow routing module within the model can be called to estimate advective exchanges between compartments. In case outflow is not monitored, a routing module is first called to solve the continuity equation for the whole wetland

$$\frac{dV}{dt} = Q_{\text{in}} - Q_{\text{out}} - ET + P - I \tag{3}$$

where dV/dt = variation of wetland storage (volume) over time ($L^3\ T^{-1}$); Q_{in} and Q_{out} = inflows and outflows, respectively, to/from the wetland ($L^3\ T^{-1}$); ET and I account for losses to evapotranspiration and infiltration, respectively ($L^3\ T^{-1}$); and P = added volume in case of direct precipitation inputs to the wetland ($L^3\ T^{-1}$). Logically, relationships explaining outflow and inundated area as functions of storage volume have to be provided to the model. The routing module is equipped with a third-order Runge–Kutta solver (Carnahan et al. 1969) for solving the continuity equation at each time step (approximately 0.01–0.1 day).

For wetlands with simple geometry where compartments are in series, a simple logic is used to calculate advective flow rates across the interface between compartments. It is assumed that the water level rises or falls simultaneously within the whole wetland (level-pool conditions); in other words, at any given time step, when inflows − outflows > 0, then all compartments will have an increase in volume of standing water; and when inflows − outflows < 0, water level in all compartments drop simultaneously. This assumption is explicitly safe to make when the kinematic wave celerity is comparable to (or larger than) the average flow velocity within the wetland. Increase or decrease in the volume of standing water in compartments will be proportional to their area, since it is assumed that depth of increase/decrease is the same for the entire wetland. At each time step, the advective exchange is estimated as the mass of water required to cause this increase/decrease of volume in each compartment. This exchange occurs between adjacent compartments, and is unidirectional. This means that over a single time step, a compartment either receives water from its immediate neighboring compartments (to gain volume), or loses water to its immediate neighbors (to lose volume).

In case of a wetland with complicated geometry, it would be best if the model is paired with a hydrodynamic model. In other words, the advective interchanges between compartments need to be provided by the user, and a hydrodynamic wetland model would be the best tool for estimating these discharges.

Diffusive/Dispersive Exchange

Diffusion and dispersion are two distinct processes that take place at very different scales. Diffusion acts at the molecular level, whereas dispersion is a macrolevel process caused by nonuniform flow patterns. Molecular diffusion happens at a rate of 10^{-8} to 10^{-4} cm^2/s, whereas dispersion has a rate of 10^4 to 10^7 cm^2/s (Chapra 1997). Hence dispersion typically overshadows molecular diffusion in aquatic environments. However, diffusion and dispersion are modeled in a similar manner, thus their effects are considered collectively in a mass transport term as dispersion/diffusion. Similar to Hantush et al. (2013), for the dispersive/diffusive mass transfer rate across the i, j boundary, $\beta_{i,j}$ can be obtained by conserving mass flow in the schematic compartmental system depicted in Fig. 2. Between two adjacent compartments (like i and 1in Fig. 2), assuming a linear drop in concentration from the center of compartment i to the interface separating the two compartments, the expression for the effective diffusive/dispersive mass transfer coefficient ($\beta_{i,j}$) can be obtained as

$$\beta_{i,1} = \frac{2\phi_1\phi_i D_1 D_i}{\phi_i D_i L_1 + \phi_1 D_1 L_i} D_i = \tau_i \times D^* \tag{4}$$

where τ_i = tortuosity of compartment i; D^* is the free-water molecular diffusion coefficient ($L^2\ T^{-1}$); ϕ_i = effective porosity of wetland surface water in compartment i; and L_1 and L_i = nonshared lengths of the two compartments, computed by dividing the area of each compartment over the shared length between the two compartments $L_i = A_i/l_{i,1}$ and $L_1 = A_1/l_{i,1}$). Initial area of each compartment as well as the length shared with adjacent compartments need to be provided by user; however, these two variables [(1) area, and (2) length, mentioned previously] shrink and expand dynamically as the total area of the wetland shrinks and expands over time, and are routinely updated at the beginning of each time step.

Several formulas have been suggested for estimation of the dispersion coefficient in streams and rivers (Chapra 1997), where

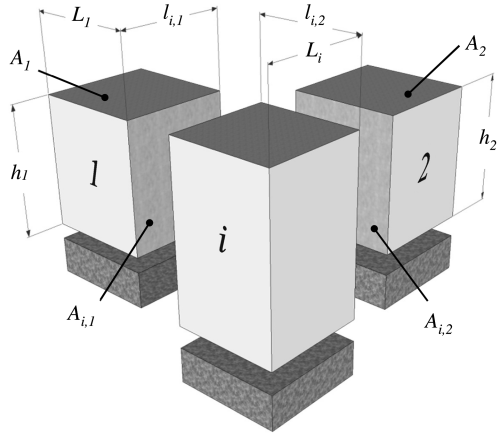

Fig. 2. Schematic illustration of three adjacent compartments and concept of effective diffusion/dispersion parameter

dispersion is computed as a function of shear velocity/discharge. Fischer (1979) have suggested the subsequent relationship for rivers

$$D_d = 0.011 \frac{U^2 B^2}{H U^*} \tag{5}$$

where D_d = dispersion coefficient ($m^2\,s^{-1}$); U = flow velocity (ms^{-1}); B = channel width (m); H = mean depth (m); and U^* = shear velocity (ms^{-1}). Shear velocity can be defined as

$$U^* = \sqrt{gHS} \tag{6}$$

where g = gravitational acceleration (ms^{-2}); and S = channel slope (dimensionless). For wetland applications, channel slope (S) should be replaced with wetland bed slope, attainable from wetland bathymetry.

In the case of hydrodynamic wetland modeling, the dispersion coefficients are generally calculated as a function of flow and grid size, multiplied by a calibration factor. The subsequent formulation, suggested by DHI (2004), is one out of several empirical methods for estimation of dispersion coefficients

$$D_x = a_x \cdot \Delta x \cdot v_x \tag{7}$$

where D_x = dispersion coefficient in x-direction ($m^2\,s^{-1}$); Δx = constant grid spacing; v_x = local current velocity in x-direction (ms^{-1}); and a_x = calibration factor.

To estimate the dispersion coefficient in *WetQual*, a combination of the two methods is utilized, such that

$$D_d = \acute{D} \times E_{\text{fact}} \tag{8}$$

where $\acute{D}$ ($m^2\,s^{-1}$) = rough estimate of the dispersion coefficient calculated through Eq. (5); E_{fact} = calibration constant; and D_d = dispersion coefficient ($m^2\,s^{-1}$). Sensitivity of the model to E_{fact} can be quantified and interpreted as a surrogate of model sensitivity to dispersion/diffusion.

Numerical Integration

Similar to previous versions of the *WetQual* model (Hantush et al. 2013; Sharifi et al. 2013), numerical integration was performed using an explicit numerical scheme with forward-difference approximation of the time derivatives.

Case Study Application

Site Description

The proposed compartmental model was applied to a restored wetland located on the west side of the San Joaquin River in California's Central Valley (Fig. 3). The materials presented in this section are adapted from Maynard (2009) and Maynard et al. (2011), who conducted research examining biogeochemical cycling and retention of carbon and nutrients in this wetland. The 4.4-ha wetland was restored in 1993 from an agricultural field with the intent of providing wildlife habitat and improving water quality of agricultural runoff. During the growing season (May–September), the wetland receives irrigation tail-water from about 2,300 ha of farmlands; whereas in winter and spring, flow is maintained by episodes of rain and flood events. Accordingly, the wetland is seasonally inundated for 9–11 months each year. The San Joaquin Valley has a Mediterranean climate with hot, arid summers ($\bar{T} = 24$°C) and cool, humid winters ($\bar{T} = 8$°C). The mean annual precipitation is 28 cm with most of the rainfall occurring between November and April. During the restoration process in 1993, the wetland surface was covered with local soil (i.e., antecedent soil layer) which had a loamy sand texture. With an average depth of 0.40 m (0.25 < depth < 0.70 m), the restored wetland had a water holding capacity of 17,684 m^3. The close vicinity of inflow and outflow structures in the northern end of the wetland leads to hydrologic short-circuiting and disconnection of the southern portion which constitutes more than 50% of the wetland area (Fig. 3). Throughout this paper, the wetland will be referred to as the San Joaquin restored wetland (SJRW).

The case study was conducted during the growing season of 2007 (late April to early September; Maynard 2009). The SJRW was monitored for flow and water quality at the inlet and outlet locations. Early spring flooding in 2007 prevented the germination of emergent macrophytes; consequently there was no emergent vegetation within the wetland during the course of the research reported in this paper. What made this site favorable for application of the proposed compartmental model is the formation of a large stagnant zone at the southern end of the wetland (Maynard 2009).

Hydrologic Balance

ISCO (ISCO, Lincoln, Nebraska) area–velocity meters were installed in inlet and outlet pipes to measure water inflow and outflow rates every 15 min. The outflow water control structure was a concrete weir box fitted with 5×15 cm (2×6 in.) flashboards for regulating the wetland water level. All water flowing over the top flashboard entered a 90-cm (36-in.) concrete culvert that was fitted with an ISCO area–velocity meter. Since field measurements of inflow and outflow discharge were available, there was no need to call the routing module. However, volume fluctuations in the wetland were calculated using the continuity Eq. (3) at a daily scale. There was no precipitation during the summer irrigation season when the research reported in this paper was conducted [i.e., $P = 0$ in Eq. (3)]. The other two parameters in Eq. (3), i.e., (1) evapotranspiration, and (2) seepage, were estimated at a daily scale. Due to the absence of plant cover in the wetland during the period of the research reported in this paper, it was assumed that transpiration was minimal and an open water evaporation rate was calculated instead of evapotranspiration. The Penman equation (Penman 1948; Dunne 1978) was employed to calculate daily evaporation rates from open water

$$E_o = \frac{H\Delta + \gamma E_a}{\Delta + \gamma} \tag{9}$$

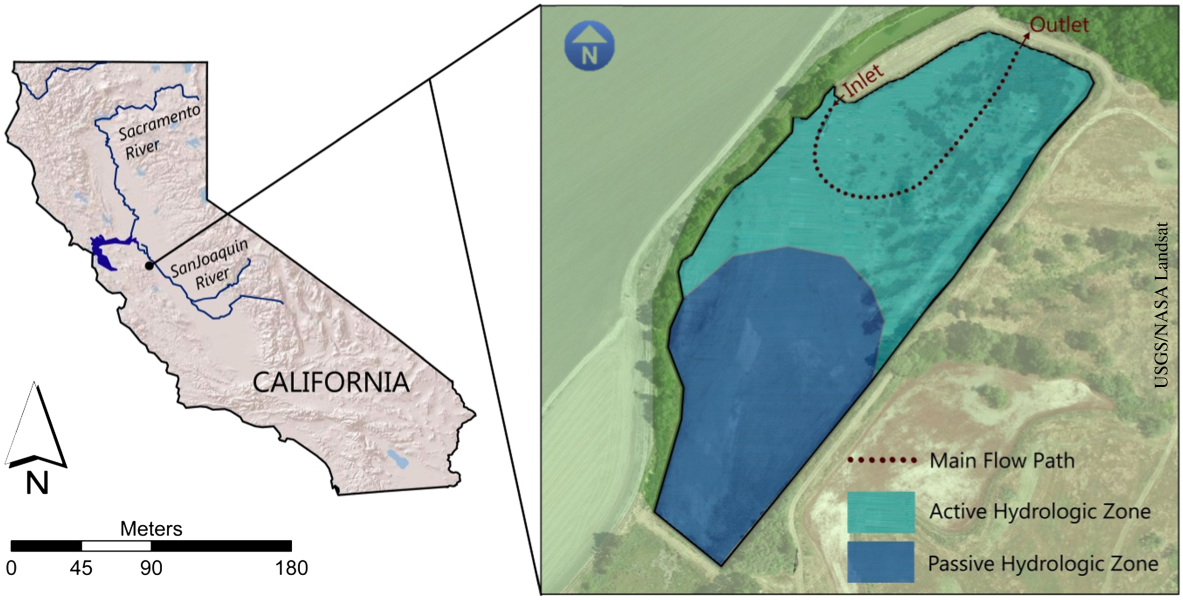

Fig. 3. Wetland investigated in the research reported in this paper, located on west side of the San Joaquin River in California's Central Valley (adapted from Maynard 2009, with permission; Landsat imagery courtesy of NASA Goddard Space Flight Center and U.S. Geological Survey)

where E_o = evaporation rate (cm/day); H = evaporation rate due to net radiation (cm/day); Δ (mb/°C) = slope of the curve relating saturation vapor pressure to temperature; γ = psychometric constant (0.66 mb/°C); and E_a = mass transfer evaporation rate. E_a is estimated by an empirical relationship suggested by Dunne (1978)

$$E_a = (0.013 + 0.00016u_2)(e_{sa} - e_a) \tag{10}$$

where u_2 = wind speed (km/day) measured at height of 2 m above the ground; e_{sa} (10^2 PA) = saturation vapor pressure at the overlaying air temperature; and e_a 10^2 PA) = atmospheric vapor pressure. The required data for estimating open water evaporation came from a nearby weather station (~15 km) at Patterson, California, maintained by CIMIS (2007). Seepage from the wetland was estimated daily by assuming that water was lost at a rate equivalent to the saturated hydraulic conductivity of the wetland soil, i.e., $Q_g = K_s \times A_w$, where K_s is saturated hydraulic conductivity (LT^{-1}); and A_w is ponded wetland area (L^2). This assumption was particularly supported for this wetland, given that the wetland is a recharging wetland, feeding an unconfined aquifer below the site.

Fig. 4 presents time series of volume and inflow/outflow discharge to/from the wetland during the irrigation season. On average, SJRW received 10,460 m^3 day^{-1} of inflow during the irrigation season (May–September) of 2007 which is equivalent to 59% of SJRW's effective water holding capacity. Consequently, this high ratio results in a relatively small residence time of 1.46 days. However, the effective residence time is actually smaller than 1.46 days due to short circuiting along the short flow path between the inlet and outlet structures. A bromide tracer experiment (conducted on August 6, 2007) demonstrated that the SJRW has an effective residence time of 0.90 day at mean inflow rates (Maynard 2009).

Water Quality Monitoring

Grab samples were collected on a weekly basis during the 2007 irrigation season from inflow and outflow locations. The samples were tested for various water quality constituents, including

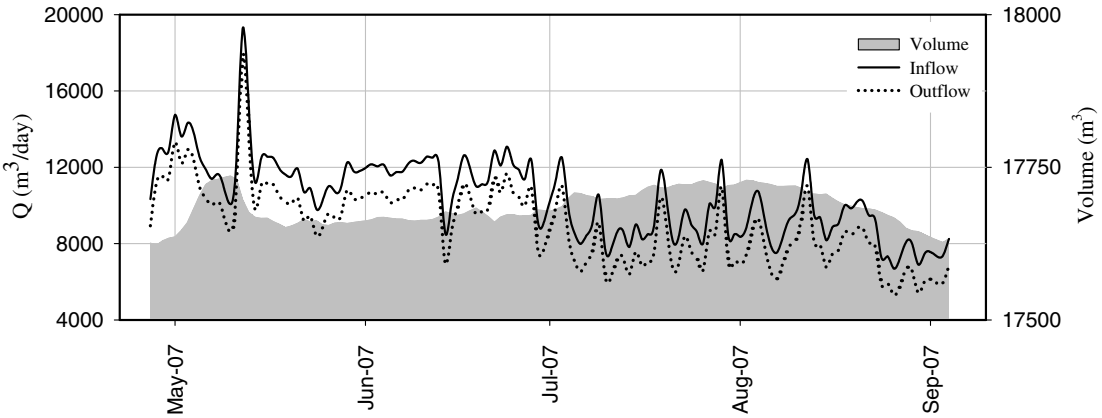

Fig. 4. Graphical demonstration of the hydrologic regime (inflow/outflow) and volume of SJRW during the growing season of 2007

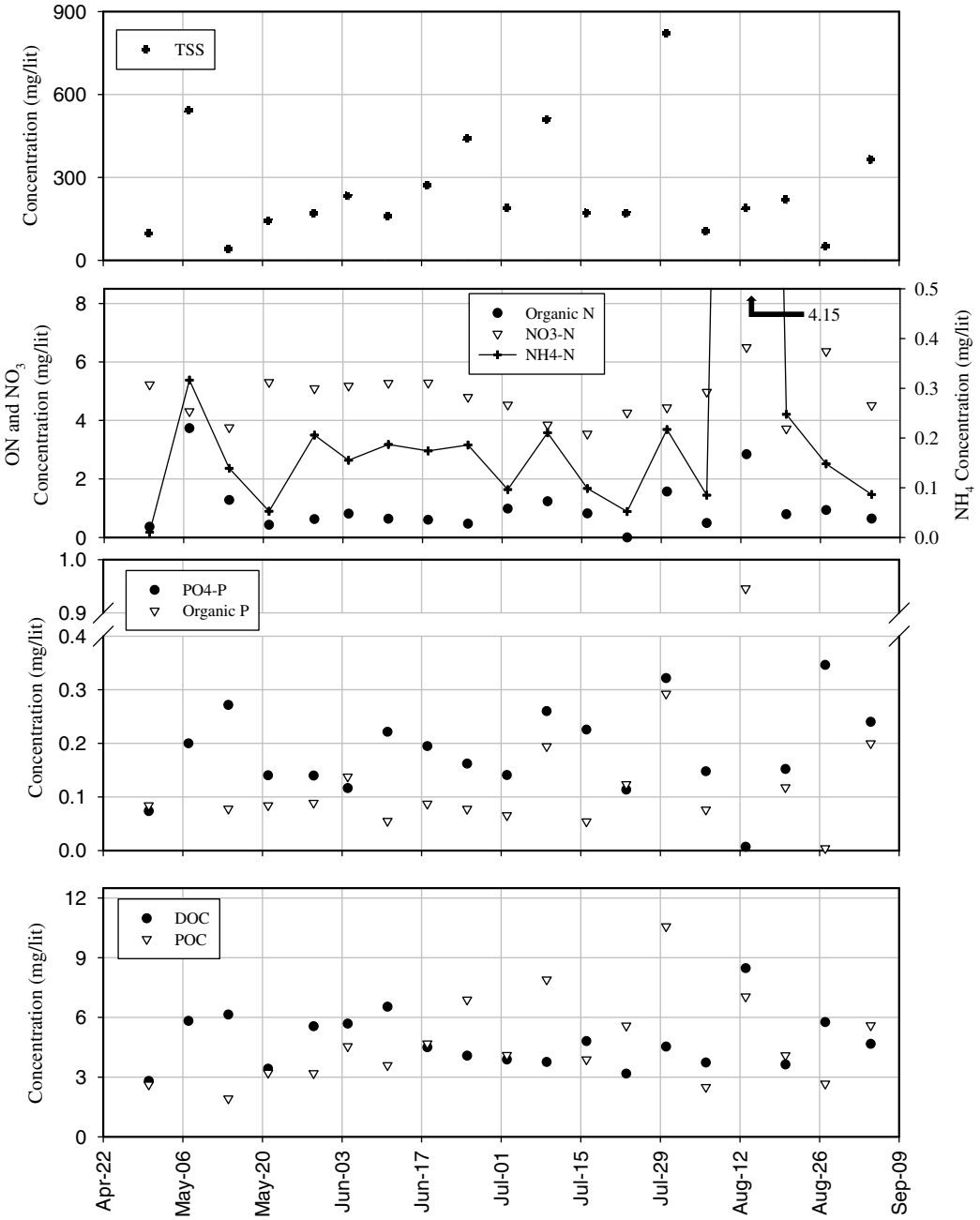

Fig. 5. Grab sample concentrations of inflow constituents to SJRW during the period of the research reported in this paper ($n = 19$)

concentrations of total suspended solids (TSSs), total nitrogen (TN), nitrate (i.e., NO_3^-), ammonia + ammonium (i.e., NH_3+NH_4^+), total phosphorus (TP), phosphate (i.e., PO_4), dissolved organic carbon (DOC), and particulate organic carbon (POC). More details on sample analysis can be found in Maynard (2009). Fig. 5 presents grab sample concentrations of inflow water constituents to SJRW during the period of the research reported in this paper ($n = 19$). Concentrations of total organic nitrogen (TON) and organic phosphorus were not directly measured; rather they were calculated by subtracting inorganic components from total nitrogen and phosphorus concentrations.

Regression Relationships for Water Quality Data at the Inlet. The model *WetQual* is a continuous model and requires continuous input data (flow and water quality) to run in a continuous mode. Much of the water quality data from SJRW was collected as weekly grab samples, i.e., only a snapshot of the inflowing pollutograph was measured with each sample. The USGS load estimator (*LOADEST*; Runkel et al. 2004) was employed to extrapolate the weekly grab sample concentration measurements to daily concentrations. By means of *LOADEST*, the user is able to develop a regression model for estimation of constituent load, based on given time series of discharge, constituent concentrations, and additional data variables (e.g., temperature). The *LOADEST* was provided with constituent concentrations collected weekly ($n = 19$) and the discharge rate at the time of sample collection, and the regression relationship with the lowest value for the Akaike information criterion (AIC) statistic (Akaike 1974) was used to make continuous (daily) time series for inflowing constituent concentrations.

For all of the constituents of interest, the same form of regression equation was identified as the best fit with the lowest AIC. The regression had the subsequent form

Table 1. Regression Statistics and Coefficient Values Generated by *LOADEST* for Constituents Inflowing to SJRW

Constituent	Regression coefficient	Coefficient value	SD	t-ratio	p-value
TSS[a]	a_0	7.38	0.25	29.18	6×10^{-17}
	a_1	1.62	0.37	4.41	1×10^{-4}
	a_2	−1.39	1.04	−1.33	2×10^{-1}
TN[b]	a_0	3.61	0.07	49.91	8×10^{-22}
	a_1	1.10	0.10	10.74	4×10^{-10}
	a_2	0.31	0.30	1.05	3×10^{-1}
NH_4-N[c]	a_0	−0.17	0.18	−0.93	3×10^{-1}
	a_1	1.80	0.26	6.88	7×10^{-7}
	a_2	0.12	0.77	0.15	9×10^{-1}
NO_3-N[d]	a_0	3.44	0.07	48.01	2×10^{-22}
	a_1	1.00	0.11	9.08	4×10^{-9}
	a_2	0.39	0.30	1.29	2×10^{-1}
TP[e]	a_0	1.02	0.12	8.48	3×10^{-8}
	a_1	0.88	0.17	5.08	2×10^{-5}
	a_2	−1.62	0.50	−3.26	2×10^{-3}
PO_4-P[f]	a_0	0.56	0.14	3.90	4×10^{-4}
	a_1	0.94	0.20	4.62	7×10^{-5}
	a_2	−1.42	0.60	−2.38	2×10^{-2}
DOC[g]	a_0	3.54	0.12	29.26	3×10^{-18}
	a_1	1.12	0.19	6.04	2×10^{-6}
	a_2	−0.43	0.51	−0.83	4×10^{-1}
POC[h]	a_0	3.63	0.16	22.55	4×10^{-15}
	a_1	1.03	0.24	4.35	1×10^{-4}
	a_2	−1.56	0.67	−2.32	2×10^{-2}

[a]$R^2 = 60.3\%$.
[b]$R^2 = 88.6\%$.
[c]$R^2 = 78.5\%$.
[d]$R^2 = 84.0\%$.
[e]$R^2 = 72.3\%$.
[f]$R^2 = 65.8\%$.
[g]$R^2 = 69.9\%$.
[h]$R^2 = 63.5\%$.

$$\ln(\text{load}) = a_0 + a_1 \ln \hat{Q} + a_2 \ln \hat{Q}^2 \tag{11}$$

where load = constituent load ($\text{kg} \cdot \text{d}^{-1}$); and $\ln \hat{Q}$ = natural logarithm of adjusted inflow, such that

$$\ln \hat{Q} = \ln Q - \left[\ln Q + \frac{\sum_{k=1}^{N} (\ln Q - \overline{\ln Q})^3}{2 \sum_{k=1}^{N} (\ln Q - \overline{\ln Q})^2} \right] \tag{12}$$

where Q = inflow (m^3/s); N = number of inflow observations in the calibration data set; and $\overline{\ln Q}$ = average natural logarithm of inflow observations (Cohn et al. 1992).

Table 1 presents the regression statistics and coefficient values for constituents of interest that were generated by *LOADEST*. The regression relationships have R^2 values ranging from 60 to 89%. Although *LOADEST* does not provide F-test statistics for the regression relationships, judging from the p-values of the coefficients, it can be stated that all regression relationships are significant at the 95% confidence level.

Prediction Intervals for Regression Relationships. Prediction intervals of the regression relationships were calculated to account for the uncertainties associated with regression relationships given by *LOADEST*. The prediction interval is a range that is likely to contain the mean response with a certain probability. The methodology for estimation of prediction intervals was adopted from Kutner et al. (2005). For a given regression relationship, the $(1 - \alpha)$ prediction limit for a new observation Y_h corresponding to X_h is estimated as

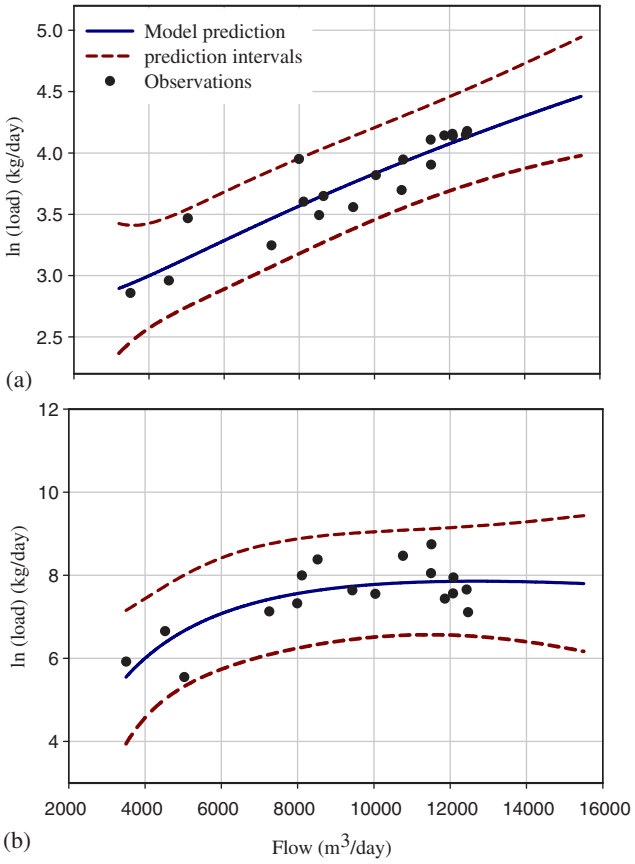

Fig. 6. Prediction intervals of regression models established for NO_3-N (top) and TSS (bottom) at 95% confidence level

$$\hat{Y}_h \pm t\left(1 - \frac{\alpha}{2}; n - p\right)\mathbf{s}(\text{pred}) \tag{13}$$

where

$$\mathbf{s}^2(\text{pred}) = \text{MSE} + \mathbf{s}^2(\hat{Y}_h) \tag{14}$$

in terms of the mean square error (MSE) of the regression model. The estimated variance $\mathbf{s}^2(\hat{Y}_h)$ is given by

$$s^2(\hat{Y}_h) = \acute{X}_h s^2(b) X_h \tag{15}$$

where $\mathbf{s}^2(b)$ = regression covariance matrix; and b = regression coefficient.

Prediction intervals for all regression relationships were calculated. Fig. 6 presents two examples [(1) NO_3^-, and (2) TSS] of regression models and their prediction intervals established for the 95% confidence level.

Compartmentalization, and Estimation of Advective Exchange between Compartments

In accordance with the compartmentalization approach, SJRW was divided into four compartments. Expert opinion of the field scientists who collected field data from SJRW was consulted in initiating the number and the boundaries of the compartments. Some level of trial-and-error was also involved in finalizing the number of compartments to be included, as a higher number of compartments add to the model uncertainty and computational costs, and too few compartments undermine the efforts for representing variability in different zones of the wetland.

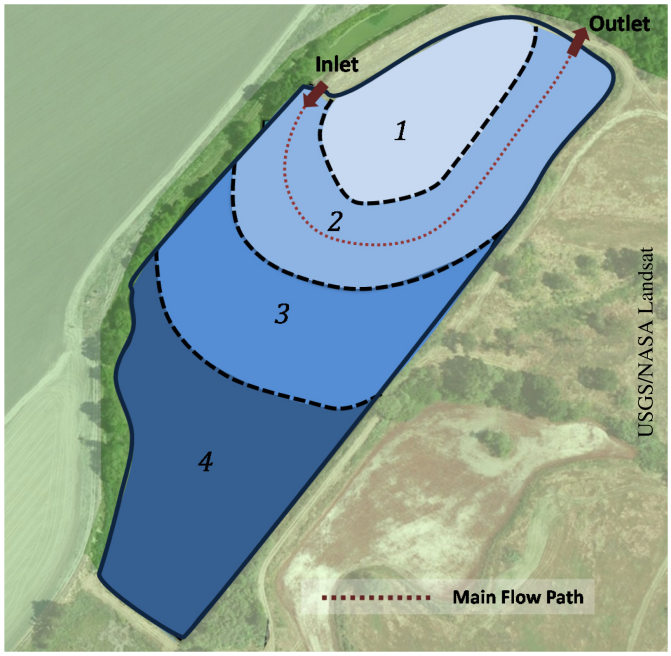

Fig. 7. Compartmentalized study wetland (Landsat imagery courtesy of NASA Goddard Space Flight Center and U.S. Geological Survey)

Table 2. Average Area, Volume, and Depth of Compartments C.1–C.4 of SJRW

Compartment attribute	C.1	C.2	C.3	C.4	Total/average
Area (m^2)	2,395	13,791	15,511	12,135	43,832
Volume (m^3)	700	3,84	5,035	8,464	17,683
Depth (m)[a]	0.29	0.25	0.32	0.70	0.40

[a]Depth = volume/area.

As shown in Fig. 7, Compartment 1 (C.1) represents a small stagnant zone formed at the north end of the wetland due to the existence of a small berm separating the main flowpath. Compartment 2 (C.2) represents the most active zone in SJRW, containing the inlet, outlet, and main flowpath. Compartments 3 and 4 (C.3 and C.4), respectively, represent the transition and stagnant zones formed at the southern end of the wetland. The SJRW deepens gradually from northeast to southwest, thus Compartment C.4 is the deepest and has the largest volume among compartments. Average area, effective volume, and depth of these compartments are presented in Table 2.

The continuity equation was solved to estimate daily volume fluctuations over the whole wetland. This variation in volume was distributed over to each compartment, according to the fraction of the total area each compartment covered. Given the simple geometry of the wetland (single inlet/outlet and compartments in series), level-pool conditions were assumed and a simple logic was used to calculate advective exchange between compartments. In this method, advective exchange at each time step was estimated equivalent to the volume of water required to impose calculated increase/decrease of volume at each compartment. Fig. 8 presents a schematic representation of the logic applied to calculate advective flux in the wetland. In a single time step, where variation in volume was positive ($\Delta V > 0$, or rising water levels), the direction of advective transfer is from Compartment C.2 outwards, such that

$$Q_{2.1} = (V^{i+1}_{w.1} - V^{i}_{w.1})/dt \tag{16a}$$

$$Q_{3.4} = (V^{i+1}_{w.4} - V^{i}_{w.4})/dt \tag{16b}$$

$$Q_{2.3} = Q_{3.4} + (V^{i+1}_{w.3} - V^{i}_{w.3})/dt \tag{16c}$$

where i = time; and $Q_{x.y}$ = advective flow rate from Compartment X to Compartment Y. Where there is a fall in water levels over one time step, the direction of advective flow will be towards Compartment C.2, such that

$$Q_{1.2} = (V^{i}_{w.1} - V^{i+1}_{w.1})/dt \tag{17a}$$

$$Q_{4.3} = (V^{i}_{w.4} - V^{i+1}_{w.4})/dt \tag{17b}$$

$$Q_{3.2} = Q_{4.3} + (V^{i}_{w.3} - V^{i+1}_{w.3})/dt \tag{17c}$$

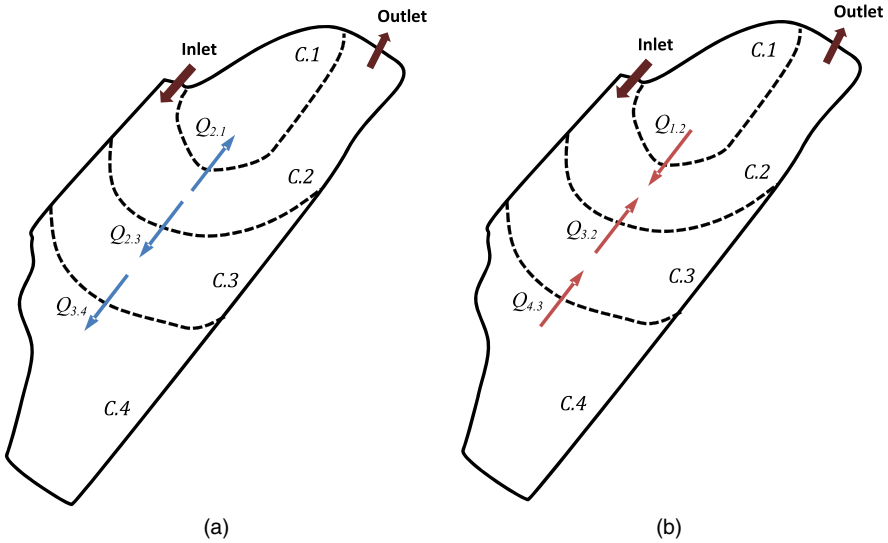

Fig. 8. Direction of advective transfer between compartments in case of the following: (a) rising water levels; (b) falling water levels

J. Hydrol. Eng.

Table 3. Definition for Model Parameters in *WetQual* Model, and Their Respective Minimum, Maximum, and Distribution

Notation	Unit	Definition	Minimum[a]	Maximum[a]	Distribution
L	cm	Thickness of active soil layer	5	50	U[b]
K_d	mL/g	Ammonium ion distribution coefficient	0.075	19.3	log-N[c]
k_{ms}	1/day	First-order slow mineralization rate in wetland soil	0.000001	0.001	log-N
k_{nw}	1/day	First-order nitrification rate in wetland free water	0.0001	0.1	log-N
k_{mw}	1/day	First-order mineralization rate in wetland free water	0.000001	0.001	log-N
k_{ns}	1/day	First-order nitrification rate in aerobic soil layer	0.01	10	log-N
k_{dn}	1/day	Denitrification rate in anaerobic soil layer (T-1)	0.004	2.6	U
a_{na}	gN/gChl	Gram of nitrogen per gram of Chlorophyll-a in plant/algae	3.5	17.6	U
$r_{c,Chl}$	gC/gChl	Carbon mass ratio in Chlorophyll a	20	100	U
S_s	g/L/day	Oxygen removal rate per unit volume of aerobic layer by other processes	0.022	0.065	U
f_r	—	Fraction of rapidly mineralizing particulate organic matter	0.5	1	U
pH	—	pH	4.5	8.2	U
a_{pa}	gP/gChl	Gram of phosphorus per gram of Chlorophyll-a	0.4	2	U
K_{sa}	cm^3/g	Phosphorus sorption distribution coefficient	10	100	log-N
K_{sb}	cm^3/g	Phosphorus precipitation with iron hydroxide distribution coefficient	100	1,000	log-N
ϕ	—	Wetland soil porosity	0.5	0.9	U
f_{Sw}	—	Fraction of nitrogen fixation in water	0.5	1	U
f_{act}	—	Vertical diffusion magnification factor	20	1,000	log-N
v_r	mm/year	Effective resuspension rate	0.0146	8.74	log-N
K_0	cm/day	Oxygen reaeration mass transfer velocity	25.60	102.02	U
k_v	cm/day	Ammonia volatilization mass transfer velocity	14.64	23.10	U
f_N	—	Fraction of total ammonia in ionized form	0.00024	1.00	U
θ	—	Temperature coefficient in Arrhenius equation	1.15	1.35	U
k_{ga}	(1/day)	Growth rate of free-floating plant	0.01	0.2	log-N
k_{gb}	(1/day)	Growth rate of benthic and rooted plant (T^{-1})	0.01	0.2	log-N
ρ_s	(g/cm^3)	Wetland soil particle density	1.5	2.2	U
v_s	(cm/day)	Effective settling velocity (LT^{-1})	0.025	25	log-N
v_b	(cm/day)	Effective burial velocity (LT^{-1})	0.000274	0.006575	U
ϕ_w	—	Effective porosity of wetland surface water	0.65	0.95	U
a_{ca}	(gC/gChl)	Ratio of carbon to Chlorophyll-a in algae	15	160	U
f_{aL}	—	Fraction of labile particulate organic carbon produced by death/loss of free floating plants and attached algae	0.01	0.99	U
f_{aR}	—	Fraction of refractory particulate organic carbon produced by death/loss of free floating plants and attached algae	0.01	0.99	U
f_{aD}	—	Fraction of dissolved organic carbon produced by death/loss of free floating plants and attached algae	0.01	0.33	U
f_{bL}	—	Fraction of labile particulate organic carbon produced by death/loss of rooted and benthic plants	0.01	0.99	U
f_{bR}	—	Fraction of refractory particulate organic carbon produced by death/loss of rooted and benthic plants	0.04	0.99	U
f_{bD}	—	Fraction of dissolved organic carbon produced by death/loss of rooted and benthic plants	0.01	0.33	U
k_L	(1/day)	First-order hydrolysis rate of labile particulate organic carbon	0.000001	0.0001	log-N
k_R	(1/day)	First-order hydrolysis rate of refractory particulate organic carbon	0.0000001	0.00001	log-N
K_O	(mg/L)	Michaelis–Menten half-saturation concentration of dissolved oxygen required for oxic respiration (ML^{-3})	0.2	1.00	U
K_O^{in}	(mg/L)	Michaelis–Menten oxygen inhabitation coefficient (ML^{-3})	0	0.51	U
K_N	(mg/L)	Michaelis–Menten nitrate nitrogen half-saturation concentration required for denitrification (ML^{-3})	0.004	0.36	log-N
K_N^{in}	(mg/L)	Michaelis–Menten nitrate-nitrogen inhibition coefficient (ML^{-3})	0.002	0.18	log-N
k_D^1	(1/day)	Maximum dissolved organic carbon utilization rate for aerobic respiration	0.0015	0.4	U
k_D^2	(1/day)	Maximum dissolved organic carbon utilization rate for denitrification	0.001	0.16	U
k_D^3	(1/day)	Maximum dissolved organic carbon utilization rate for methanogenesis	0.0005	0.08	U
k_M^1	(1/day)	Maximum methane utilization rate for aerobic respiration	0.001	0.25	U
k_M^2	(1/day)	Maximum methane utilization rate for denitrification	0.001	0.08	U
f_{bw}	—	Fraction of rooted plant biomass above soil–water interface	0.4	0.7	U
E_{fact}	—	Magnification parameter for the processes of horizontal diffusion and dispersion between compartments	0.0	0.1	log-N

[a]The selected range values for the listed parameters/coefficients are from soft information (i.e., literature tabulation and expert knowledge), e.g., Kadlec and Hammer (1988), Schnoor (1996), Chapra (1997), Di Toro (2001), Jrgensen and Bendoricchio (2001), Pivato and Raga (2006), Liang et al. (2007), Reddy and Delaune (2008), Cerco and Cole (1995), and Ji (2008).

[b]Uniform distribution.

[c]Log–normal distribution; lower and upper bounds in log-N distributions refer to values corresponding to probabilities of 0.1 and 99.9%, respectively.

Table 4. Average Model Performances for Behavioral Simulations Based on Observed and Simulated Concentrations

Goodness of fit	PO_4	TN	ON	NH_4^+	NO_3^-	TSS	TOC
E_{NS}	−0.03	0.41	0.22	0.14	0.58	−0.22	0.62
MBE (%)	−0.41	0.29	0.15	−0.07	0.52	−0.33	0.57

Model Assessment

Model assessment performed in the research reported in this paper was similar to that described in Sharifi et al. (2013). A combination of both generalized likelihood uncertainty estimation (GLUE) and global sensitivity analysis (GSA) techniques (Beven and Binley 1992; Spear and Hornberger 1980) were employed to assess model prediction uncertainty and quantitative sensitivity to model parameters. In brief, 100,000 statistically independent parameter sets were generated for each compartment as sampled randomly from previously selected prior distributions which were extracted from literature values/tabulations. Model parameter distribution and their respective upper and lower bounds (quantities) for carbon, nitrogen, phosphorus, and sediment cycles can be found in Table 3. To perform Monte Carlo (MC) simulations, the model was run 100,000 times, each time with one set of parameters to yield an ensemble of 100,000 time series for constituent concentrations. At the beginning of each run, a module within the model generates water inflow concentrations for TSS, TN, NH_4^+, NO_3^-, TP, PO_4, DOC, and POC to SJRW for the dates with no observed data. These time series were different from one model run to another, since inflow concentrations were generated randomly within the 95% prediction intervals of the developed regression models. In this manner, uncertainty in the water inflow concentrations was accounted for in the GLUE and GSA analysis.

Two performance criteria [(1) mass balance error (MBE), and (2) Nash–Sutcliffe efficiency (E_{NS})] were used to construct a performance measure that evaluates the goodness-of-fit between model-predicted concentrations and observed data for each MC simulation such that

$$L_k = 0.5 \times \left[(E_{\mathrm{NS}} + \exp\left(\frac{-|\mathrm{MBE}|}{100}\right)\right] \tag{18}$$

The performance measure L_k can theoretically range between $-\infty$ and 1. Such a measure enables capturing goodness-of-fit for both average constituent concentrations and their variation over time. For each compartment, parameter sets were sorted based on their performances and the top 1% of datasets with the highest performances were separated as the behavioral dataset (B) from the rest of the parameter sets (nonbehavioral datasets, B').

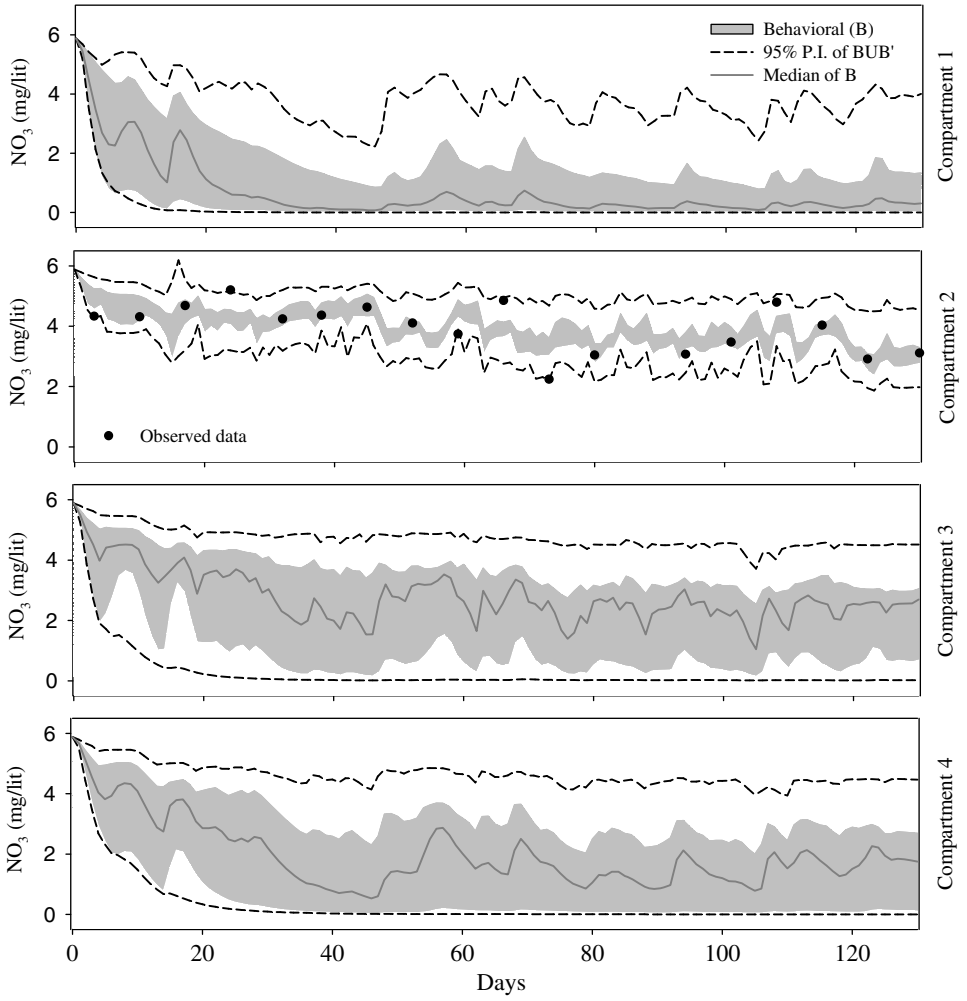

Fig. 9. Model-generated 95% prediction intervals (PI) from 100,000 MC simulations versus observed concentrations of NO_3^- for Compartments C.1–C.4

Subsequently, quantitative sensitivity analysis was performed using the Kolmogorov–Smirnov (K–S) test (Massey 1951) to reveal the most sensitive parameters. The Kolmogorov–Smirnov test is a nonparametric test that is used to quantify a distance between the reference cumulative distribution function (CDF), generated for each parameter from nonbehavioral parameter values or B', and the CDF of a parameter generated from the behavioral datasets (or B). If such distance, referred to as $D_{\max}$, is significant at a certain confidence level (α), the parameter is declared sensitive. Prior and posterior prediction uncertainty were next obtained by using model predictions generated respectively from the whole spectrum of model parameter distributions (B, U, and B'), and from behavioral parameters only (B).

Results and Discussion

Model fitness was gauged by comparing simulated concentrations of TSS, TN, NO_3^-, TON, NH_4^+, TOC, and PO_4 with observed data collected at the SJRW outlet ($n = 19$) using two performance criteria of (1) mass balance error, and (2) Nash–Sutcliffe efficiency.

Table 4 exhibits average model performances (E_{NS} and MBE) for behavioral simulations. Judging from these data, the model performed fairly well capturing TOC dynamics, with an average E_{NS} of 0.62 and a mass balance error of less than 1%. In general mass balance error was very small (<1%) for all predicted constituents. The model performed well in predicting nitrogen dynamics within the wetland investigated in the research reported in this paper, with TN having an average E_{NS} of 0.41. Within the nirtogen cycle, the best performance was associated with NO_3^- ($E_{NS} = 0.58$). Unfortunately, model performance for PO_4 and TSS were not acceptable, as indicated by negative E_{NS} values. Thus for the rest of the Results section, attention will be focused on model outcomes associated with carbon-related and nitrogen-related constituents.

Uncertainty Analysis

Figs. 9–11, respectively, compare the observed concentrations of NO_3^-, TN, and TOC with the model results generated from the behavioral dataset and the 95% prediction interval (a band that on average encompasses 95% of the predicted values) of the MC simulations. What is commonly observed in Figs. 9–11 is that Compartment C.2 has the lowest posterior uncertainty among all compartments. This observation is expected as the observed constituent concentrations (shown with black dots in Figs. 9–11) were sampled from the wetland outlet which is located in Compartment C.2. Consequently model validation was performed using model outcomes from Compartment C.2. In other words, Compartment C.2 is the most important compartment influencing model fitness and consequently it has the smallest uncertainty among all compartments.

Nitrate concentrations in Compartments C.1, C.3, and C.4 declined initially and stabilized around Day 50 (Fig. 9). It could be interpreted that the initial concentrations set for these

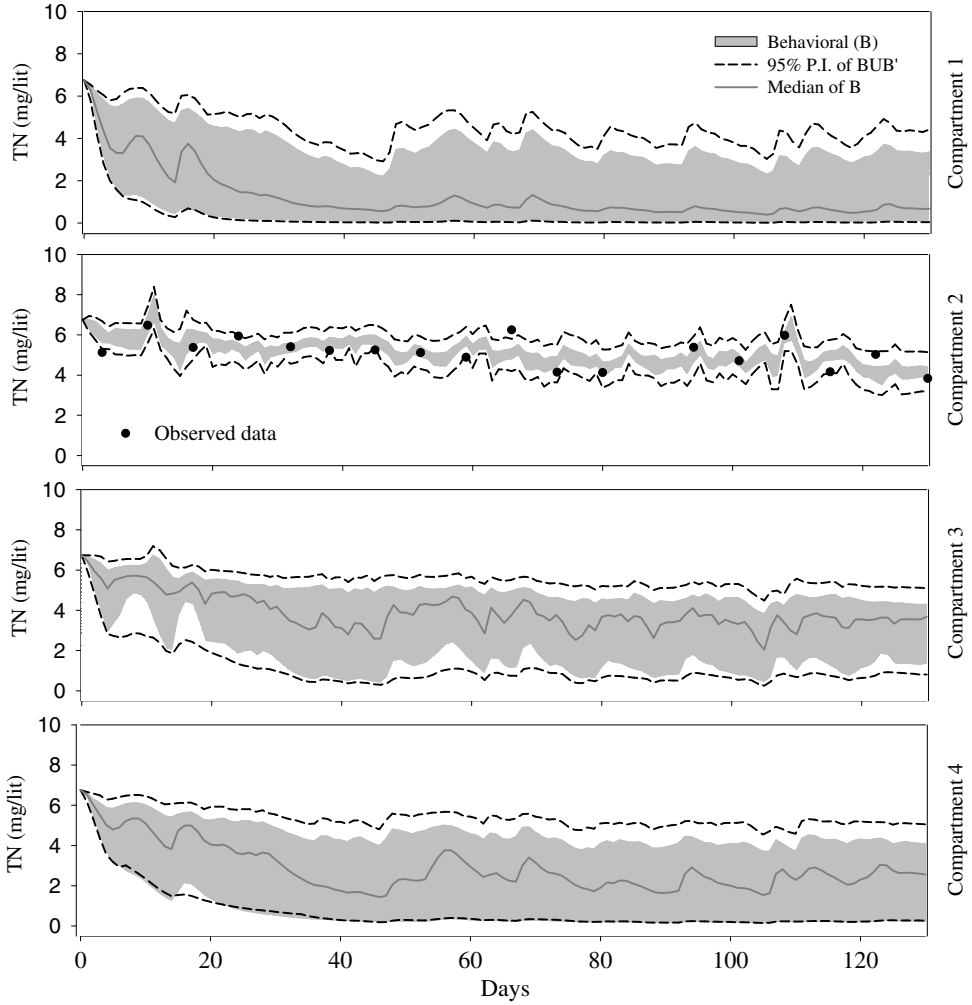

Fig. 10. Model-generated 95% prediction intervals from 100,000 MC simulations versus observed concentrations of TN for Compartments C.1–C.4

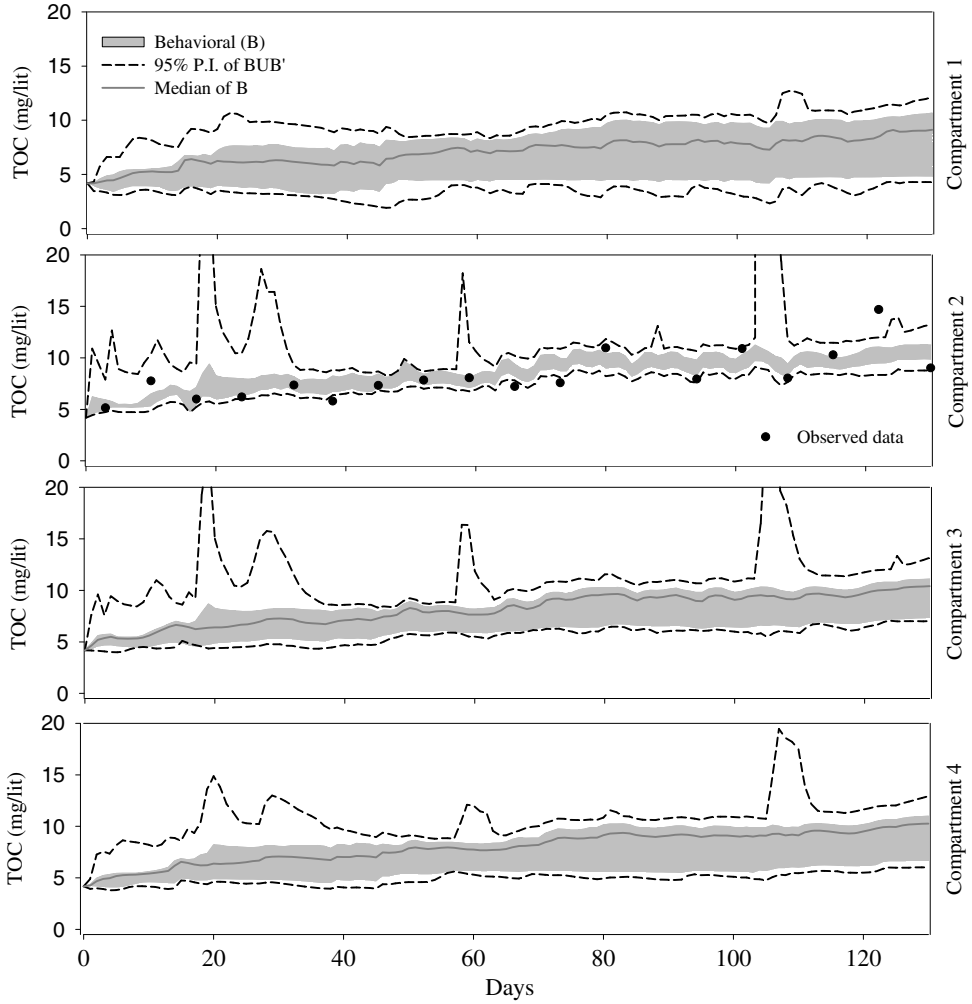

Fig. 11. Model-generated 95% prediction intervals from 100,000 MC simulations versus observed concentrations of TOC for Compartments C.1–C.4

compartments (6 mg/L, assumed ≈ average inflow concentration of NO_3^-) was originally high and better results may have been achieved if the initial concentration uncertainty was considered. This same phenomenon was observed for TN (Fig. 10). Except for a few unexpected (and unexplainable) peaks, uncertainty bands for TOC are generally narrower compared to TN and NO_3^-, indicating less uncertainty in TOC predictions. Another observation from Fig. 11 is that TOC concentration increases over time and uncertainty bands in all compartments grew wider along with it. In other words, the model exhibits higher prediction uncertainty with higher TOC concentrations. However, this is not the case with NO_3^- and TN predictions, as uncertainty remains more or less constant, even as concentrations drop over time.

Sensitivity Analysis

Figs. 12 and 13 summarize the most sensitive parameters for all compartments of the wetland in order of sensitivity based on TN and TOC export, respectively. On the vertical axes of the graphs is D_{max} from the K–S test and the most sensitive parameters are listed on the horizontal axis in order of sensitivity. Definitions for these parameters are found in Table 3. The confidence level was set at $P < 0.10$ as opposed to previous *WetQual* application studies (Sharifi et al. 2013; Kalin et al. 2013), because few parameters were sensitive at the $p < 0.05$ confidence level. The reason behind this observation may be attributed to limited observation data for validation and to a large pool of model parameters. Compared to a lumped model (single compartment model), the compartmentalized model has 4 times more parameters, but the same number of observation points (concentrations measured at the outflow, $n = 19$). Through Figs. 12 and 13, it is possible to predict which processes are important in the whole wetland, and which processes gain importance along the activity gradient line, from active to passive zones, regarding nitrogen and carbon constituents within the wetland. The reader is referred to Table 5 for complete results of the K–S test for different constituents (TON, NH_4^+, NO_3^-, TN, and TOC) in Compartments C.1–C.4.

Dispersive/Diffusive Exchange. The dispersion coefficient is known to be one of the most important parameters in advection–dispersion simulations of hydrodynamic models (DHI 2004). This was also the case for this compartmental model. The K–S test performed based on model performance for TOC and TN export revealed that the most sensitive parameter for all compartments in the wetland was E_{fact} (magnification parameter for horizontal diffusion and dispersion between compartments). As mentioned previously, at the beginning of each time step, the model computes a rough estimate of the dispersion coefficient using Eq. (5), and then multiplies it by E_{fact} In other words, E_{fact} is a magnification parameter for the processes of horizontal diffusion and dispersion between compartments. The term E_{fact} had a large

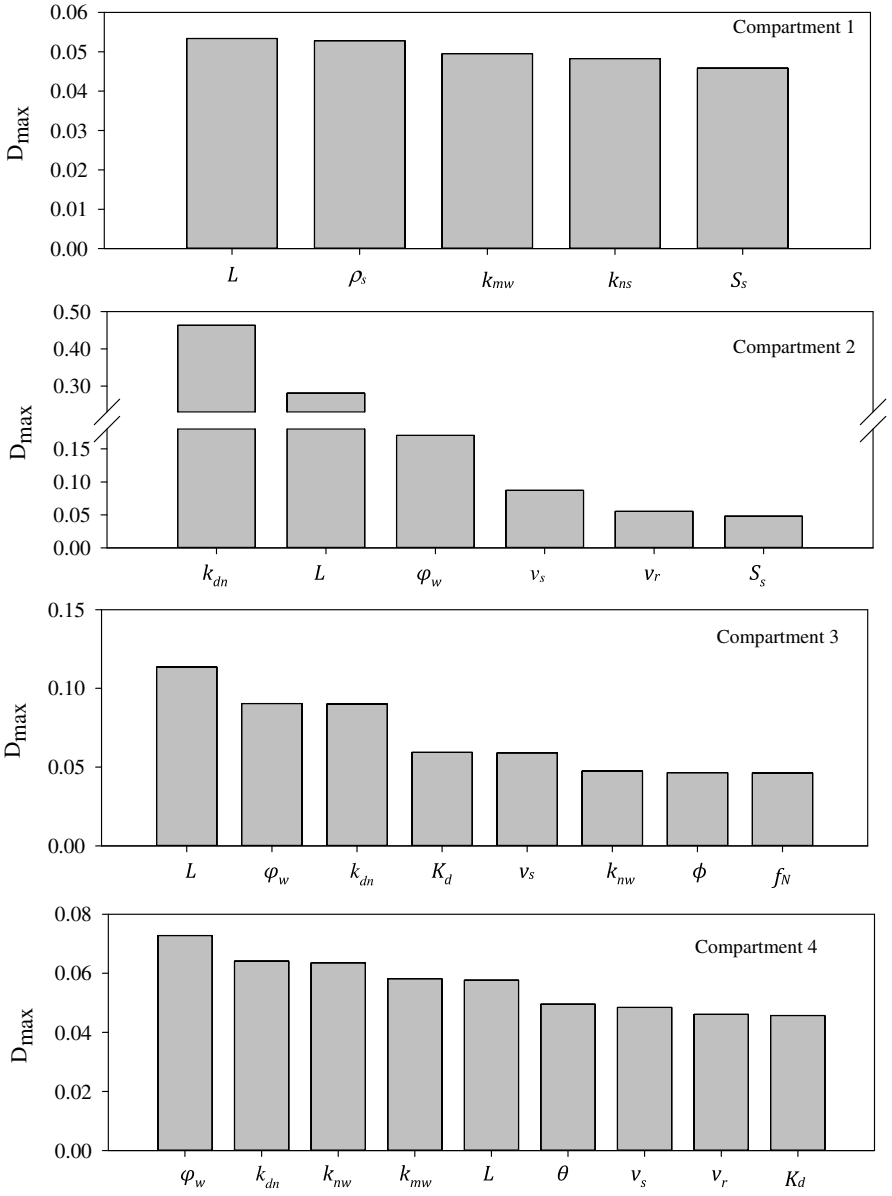

Fig. 12. Summary of the K–S test and order of sensitivities based on TN export for compartments C.1–C.4; refer to Table 3 for definition of the parameters

$D_{\max}$ (ranging from 0.29 to 0.69) and a very small p-value (in cases close to 1×10^{-41}) for every K–S test performed throughout the research reported in this paper. Since the $D_{\max}$ associated with E_{fact} dwarfed all other parameters, it was eliminated from Figs. 12 and 13.

Total Nitrogen. Fig. 12 presents a summary of the K–S test and order of sensitivities for all compartments of the wetland based on TN export. Parameter k_{dn}, representing denitrification rate, repeatedly shows up as an important parameter for Compartments C.2–C.4. Accordingly, it could be said that denitrification is an important loss pathway for nitrogen in the entire wetland (except for Compartment C.1). Parameters L and ϕ_w also repeatedly show up as sensitive parameters, indicating that having an accurate estimation of the active sediment layer depth and effective porosity of the wetland surface water is very important for successful model application.

Parameters v_s and v_r, which reflect settling and resuspension velocities, respectively, appear higher in sensitivity order at the active zone (Compartment C.2) compared to transition and stagnant zones (Compartments C.3 and C.4). An explanation for this could be that since both inlet and outlet locations of the wetland are in Compartment C.2, a large portion of particles entering the wetland settle in Compartment 2 before being transferred to other compartments, or exiting the wetland. Also because of the relatively high velocities within the active zone due to large inflow/outflow rates, resuspension will be more important compared to stagnant zones.

Total Organic Carbon. Fig. 13 presents a summary of the K–S test and order of sensitivities based on TOC export for all compartments of the wetland. Decomposition of DOC appears to be the dominant process within the entire wetland investigated in the research reported in this paper, as parameters k_D^1, k_D^2, and k_D^3 (maximum dissolved organic carbon utilization rate for, respectively, aerobic respiration, denitrification, and methanogenesis) appear at the top of the sensitivity list for all compartments. This finding is not surprising as 45% of the TOC pool is comprised of DOC. Parameters v_s and ϕ_w, respectively, representing velocity of settling

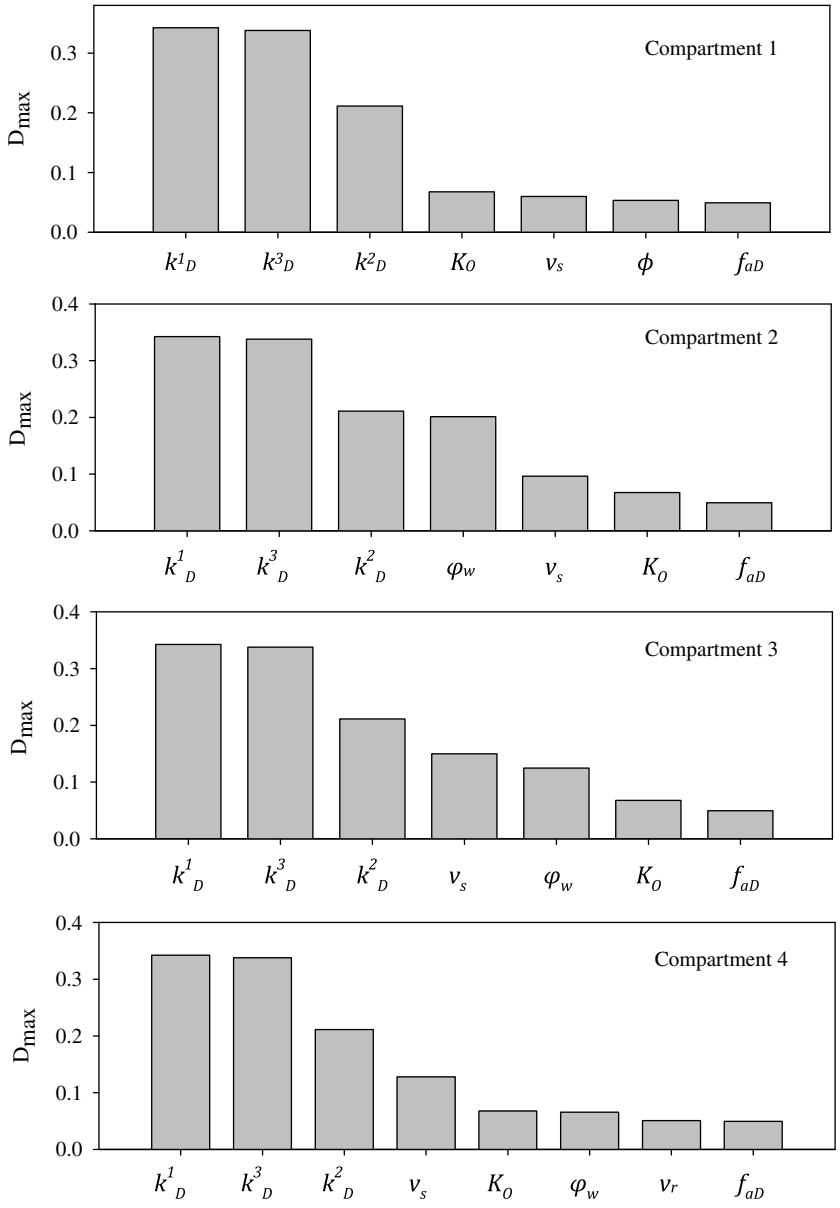

Fig. 13. Summary of the K–S test and order of sensitivities based on TOC export for compartments C.1–C.4; refer to Table 3 for definition of the parameters

and effective porosity of wetland surface water appear as important parameters for all compartments. The term ϕ_w was employed in the model to represent the effect of plant biomass occupying part of the submerged wetland volume. The term ϕ_w is signified as an important parameter despite the fact that there were no plants present during the period of the research reported in this paper. This suggests that there are inaccuracies involved in determination of the active volume estimation and the model is taking advantage of ϕ_w to adjust the wetland volume, which was given as an input. In other words, having an accurate estimate of the wetland active volume is essential for a successful modeling outcome.

There is no indication of one specific parameter/process being most important for TOC export along the active/passive zone pathway according to K–S test results. One reason behind this might be the lack of data availability for all the compartments of the wetland. Currently, the fitness of the model is gauged based on observed concentrations available for Compartment C.2. In other words, posterior distribution of parameters (required for K–S test) in all compartments was obtained by information that was only available from Compartment 2. An ideal situation would require all compartments to have their own time series of observed concentration, so that the posterior distribution of parameters for each compartment is derived solely on information from that compartment. Thus, if concentration data were available for all compartments, different parameters may have been sensitive for different compartments. It is possible that expanding the sensitivity analysis by using other techniques that do not require observed data, such as global sensitivity analysis (GLoSA) (Haan 2002), can be helpful in circumstances where the availability of observed data is limited. Another explanation may be that in the case of TOC export, the system is more or less uniform. In other words, important processes regarding TOC export are similar in all compartments.

Mass Balance Analysis

Tables 6 and 7 summarize the nitrogen and carbon budgets and the major retention and removal pathways for Compartments C.1–C.4

Table 5. Results of K–S Test (D_{max}) for Different Constituents at Compartments C.1–C.4

	Total organic N				Ammonia-N				Nitrate-N				Total N				Total organic C			
Parameter	C.1	C.2	C.3	C.4	C.1	C.2	C.3	C.4	C.1	C.2	C.3	C.4	C.1	C.2	C.3	C.4	C.1	C.2	C.3	C.4
L	0.042	0.036	**0.060** [a]	0.026	0.038	0.034	**0.084**	**0.054**	**0.056**	**0.298**	**0.052**	0.035	**0.053**	**0.281**	**0.114**	**0.058**	0.022	0.041	0.035	0.044
K_d	0.020	0.029	0.028	0.032	0.025	**0.090**	**0.074**	0.041	0.038	0.029	**0.047**	0.023	0.035	0.040	**0.059**	**0.046**	[b]			
k_{ms}	0.030	0.023	0.038	0.030	0.016	**0.076**	**0.057**	**0.060**	0.037	0.021	0.035	0.029	0.024	0.038	0.037	0.040				
k_{nw}	0.016	0.035	0.033	0.024	0.024	0.021	**0.046**	0.040	0.021	0.030	**0.048**	0.024	0.020	0.032	**0.048**	**0.064**				
k_{mw}	0.031	0.034	0.028	0.019	0.035	0.038	0.029	**0.050**	0.021	0.016	**0.048**	0.043	**0.050**	0.036	0.023	**0.058**				
k_{ns}	0.040	0.035	0.020	**0.047**	0.031	0.036	0.032	0.020	0.024	0.031	0.032	0.036	**0.048**	0.042	0.024	0.042				
k_{dn}	0.027	0.029	0.025	0.021	0.029	0.018	0.029	0.033	0.035	**0.310**	0.045	0.034	0.031	**0.464**	**0.090**	**0.064**				
a_{na}	0.023	0.032	**0.064**	0.036	0.029	0.031	0.033	0.033	**0.047**	0.029	0.034	0.032	0.044	0.026	0.025	0.028				
$r_{c,chl}$	0.031	0.021	0.026	0.018	0.045	0.033	0.031	0.037	0.039	0.030	0.024	0.030	0.043	0.029	0.035	0.027	0.023	0.046	0.022	0.024
S_s	0.021	0.043	0.028	0.030	**0.047**	**0.052**	0.045	0.021	0.028	0.029	**0.047**	0.029	**0.046**	**0.048**	0.015	0.024	0.042	0.039	0.026	0.026
f_r	0.042	0.029	0.017	**0.059**	0.027	0.029	0.036	0.035	0.021	0.038	0.033	**0.062**	0.028	0.026	0.029	0.033	0.025	0.029	0.029	0.032
pH	0.022	0.035	**0.048**	0.024	0.021	0.041	0.030	0.027	**0.050**	0.042	0.040	0.023	0.045	0.028	0.037	0.031	0.024	0.019	0.029	0.022
ϕ	**0.060**	**0.049**	0.044	0.030	0.040	0.034	0.033	0.027	0.036	0.033	0.033	0.037	0.017	0.035	**0.046**	0.034	**0.053**	0.025	0.027	0.023
f_{sw}	0.030	0.040	0.036	0.023	**0.059**	0.043	0.026	0.038	0.023	0.034	0.041	0.029	0.023	0.040	0.037	0.024				
f_{act}	0.034	0.031	0.030	0.029	0.021	0.034	0.025	0.031	0.021	0.022	0.033	0.022	0.033	0.033	0.038	0.026	0.027	0.035	0.020	0.044
v_r	0.033	0.101	0.030	0.035	0.035	0.053	0.037	0.035	0.043	0.043	0.034	0.045	0.041	**0.055**	0.046	**0.046**	0.032	0.055	0.027	**0.051**
K_0	0.032	**0.050**	0.037	0.033	0.030	0.033	**0.053**	**0.055**	0.021	0.036	0.029	0.038	0.035	0.023	0.039	0.036				
k_v	0.032	**0.050**	0.037	0.033	0.030	0.033	**0.053**	**0.055**	0.021	0.036	0.029	0.038	0.035	0.023	0.039	0.036				
f_N	0.022	0.040	0.030	0.037	0.042	0.027	0.039	0.020	0.031	0.039	0.041	0.032	0.024	0.036	**0.046**	0.029	0.029	0.024	0.040	0.027
θ	**0.062**	**0.051**	**0.056**	0.029	0.020	0.027	0.021	0.031	**0.048**	**0.055**	0.029	0.032	0.043	0.026	0.022	**0.050**	0.042	0.026	0.035	0.044
k_{ga}	0.023	0.030	0.041	**0.067**	0.018	0.023	0.037	0.021	0.041	0.033	0.029	0.026	0.028	0.035	0.032	0.024	0.036	0.024	0.045	0.025
k_{gb}	0.027	0.037	0.037	0.020	0.045	**0.048**	0.045	0.027	0.045	0.028	**0.056**	0.029	0.028	0.025	0.033	0.045	0.027	0.020	0.022	0.020
ρ_s	0.025	0.028	0.037	0.026	0.021	0.017	**0.046**	0.044	0.019	0.040	0.020	0.034	**0.053**	0.039	0.026	0.036	0.028	0.031	0.036	0.032
v_s	0.032	0.069	0.349	0.092	0.037	0.037	0.051	0.039	0.038	0.039	0.031	0.052	0.037	**0.087**	0.059	**0.048**	**0.060**	**0.096**	**0.150**	**0.128**
v_b	0.034	0.027	0.028	0.030	**0.050**	0.037	0.025	0.022	0.027	0.022	0.033	0.027	0.026	0.022	0.042	0.031	0.022	0.027	0.022	0.026
ϕ_w	0.039	**0.126**	**0.115**	**0.048**	0.040	**0.167**	**0.151**	0.044	0.034	**0.047**	0.044	**0.060**	0.033	**0.170**	**0.090**	**0.073**	0.032	**0.201**	**0.125**	**0.066**
a_{ca}																	0.039	0.039	0.039	0.039
f_{aL}																	0.024	0.024	0.024	0.024
f_{aR}																	0.025	0.025	0.025	0.025
f_{aD}																	**0.049**	**0.049**	**0.049**	**0.049**
f_{bL}																	0.030	0.030	0.030	0.030
f_{bR}																	0.045	0.045	0.045	0.045
f_{bD}																	0.022	0.022	0.022	0.022
k_L																	0.039	0.039	0.039	0.039
k_R																	0.029	0.029	0.029	0.029
K_O																	**0.068**	**0.068**	**0.068**	**0.068**
K_O^{in}																	0.040	0.040	0.040	0.040
K_N																	0.045	0.045	0.045	0.045
K_N^{in}																	0.033	0.033	0.033	0.033
k_D^1																	**0.338**	**0.338**	**0.338**	**0.338**
k_D^2																	**0.211**	**0.211**	**0.211**	**0.211**
k_D^3																	**0.248**	**0.248**	**0.248**	**0.248**
k_M^1																	0.022	0.022	0.022	0.022
k_M^2																	0.043	0.043	0.043	0.043
f_{bw}																	0.016	0.016	0.016	0.016
E_{fact}	**0.687**	**0.687**	**0.687**	**0.687**	**0.297**	**0.297**	**0.297**	**0.297**	**0.436**	**0.436**	**0.436**	**0.436**	**0.687**	**0.687**	**0.687**	**0.687**	**0.643**	**0.643**	**0.643**	**0.643**

[a]Bold digits represent sensitive test results at $P < 0.10$ confidence level.

[b]Blank values convey that the parameter is not directly or indirectly involved in the simulation of that constituent.

Table 6. Nitrogen Budget in SJRW

Budget component	C.1	C.2	C.3	C.4	Total[a]
Runoff	0	7,921.3 ± 120.1	0	0	7,921.3 ± 120.1 100 ± 1.5
Outflow	0	6,069.5 ± 188.6	0	0	6,069.5 ± 188.6 76.6 ± 2.3
Net deposition	0.7 ± 0.4	14.4 ± 22.1	11.9 ± 10.7	7.7 ± 6.1	34.7 ± 38.3 0.4 ± 0.5
Volatilization	0.1 ± 0.1	1.3 ± 2.2	1.1 ± 1.8	0.7 ± 1.1	3.2 ± 5.2 0.0 ± 0.1
Denitrification	37.6 ± 21.9	1,342.8 ± 396.3	871.6 ± 359.4	419.4 ± 213.6	2,671.4 ± 991.2 33.7 ± 12.5
NH_4^+ diffusion	−0.2 ± 0.1	0.2 ± 0.9	0.1 ± 0.7	−0.1 ± 0.4	0.0 ± 2.0 0.0 ± 0.0
NO_3^- diffusion	9.5 ± 5.5	773.1 ± 139.9	396.0 ± 108.2	144.6 ± 56.4	1,322.7 ± 310.0 16.7 ± 3.9
Seepage, GW loss	7.0 ± 2.7	216.1 ± 4.6	170.4 ± 25.4	95.0 ± 23.7	488.5 ± 56.4 6.2 ± 0.7

Note: All values, except where noted, are in kilograms.
[a]The values in each cell after the line break are normalized percentages with runoff TN loading.

Table 7. Carbon Budgets in SJRW

Budget component	C.1	C.2	C.3	C.4	Total[a]
Runoff	0	11,861.3 ± 82.2	0	0	11,861.3 ± 82.2 100 ± 0.7
Outflow	0	9,352.8 ± 436.5	0	0	9,352.8 ± 436.5 78.8 ± 3.7
Aerobic respiration	1.6 ± 1.5	234.4 ± 158.8	125.4 ± 99.4	63.4 ± 63	424.8 ± 322.7 3.6 ± 2.7
Anaerobic respiration	15 ± 13.4	109.7 ± 82.3	133.8 ± 98.9	87.6 ± 67.3	346.1 ± 261.9 2.9 ± 2.2
Deposition	12 ± 14.2	78.3 ± 128.4	79.8 ± 92.2	72.0 ± 105.9	242.1 ± 340.7 2.0 ± 2.9
Diffusion	12.5 ± 7.8	98.0 ± 60	110.3 ± 65.8	65.7 ± 37.6	286.5 ± 171.2 2.4 ± 1.4
Seepage, GW loss	32.1 ± 1.8	188.2 ± 11.9	211.1 ± 13.1	164.5 ± 10	595.9 ± 36.8 5.0 ± 0.3

Note: All values, except where noted, are in kilograms.
[a]The values in each cell after the line break are normalized percentages with runoff TN loading.

and for the whole wetland during the period of the research reported in this paper. In the last column of Tables 6 and 7, the numbers are normalized with the incoming load (shown after the line break in each cell) to demonstrate a better picture of all the sources and sinks relative to loading. Values shown are the means plus or minus one SD obtained from the behavioral set simulations.

Over the course of the period of the research reported in this paper, about 23.4 ± 3.9% (1,852 ± 309 kg) of the incoming TN load was removed or retained by SJRW, mainly through the processes of denitrification and diffusion of nitrate into wetland soil. Among the removal/retention processes, denitrification was prominent in removing 2,671.4 ± 991.2 kg (33.7 ± 12.5%) of the NO_3^- pool. Next in importance was diffusion of NO_3^- from water to soil layers which retained 1,322.7 ± 310.0 kg (16.7 ± 3.9%) of the NO_3^- pool. Surprisingly, net deposition of ON plays a very small role in removal of nitrogen with 34.7 ± 38.3 kg (0.4 ± 0.5%). These data point to the importance of nitrate in the nitrogen cycle of SJRW which is not unexpected since 70% of the SJRW TN pool was comprised of NO_3^- during the period of the research reported in this paper. The summarized nitrogen budget in Table 6 is not a closed budget and there is an apparent mass balance error. In other words, the difference between inflow and outflow mass of nitrogen (net reduction = inflow − outflow) is much smaller than mass of nitrogen removed/retained by deposition, diffusion, denitrification, volatilization, and seepage [groundwater (GW) loss]. This error partly stems from the high uncertainty involved in estimation of inflow concentrations (inflow uncertainty) and model parameters (parameter uncertainty). Another source of error in mass balance calculations is the double counting of NO_3^- retained by diffusion and removed by denitrification + seepage. Diffusion is an internal exchange pathway and not a system loss pathway. Denitrification occurs in the anaerobic sediment layer, thus nitrate has to diffuse into the soil first, before being denitrified. Also nitrate and ammonia diffuse to lower soil layers before leaving the system through seepage. Consequently, to avoid double counting, the part of the nitrate pool that diffuses into the soil but is later lost through denitrification and seepage should not be considered in mass balance error calculations.

The uncertainty associated with inflow loads is relatively small (1.5%) compared to uncertainties involving model processes (like denitrification). Denitrification, as the most important nitrogen removal process, has the highest uncertainty (largest SD). This

indicates that specific attention should be given to estimation of parameters related to the denitrification processes.

Moving from the active to passive zones of the wetland (Compartments C.2–C.4) it is generally observed that mass of all exchanges (physical and biogeochemical) decrease along the activity gradient. Concentrations of TN and NO_3^- are generally smaller in the passive zone (Compartment C.4) compared to active zone (Compartment C.2), thus one can expect all mass exchanges in Compartment C.4 to be smaller than Compartment C.2. However, there are indications in Table 6 that point to higher denitrification reaction rates in Compartment C.4 compared to Compartment C.2. The ratio of denitrification to NO_3^- diffusion in each compartment (α_i = mass of dinitrification in C_i/mass of diffusion in C_i), grows larger in passive zones compared to active zones ($\alpha_2 = 1.7 \pm 2.8$, $\alpha_3 = 2.2 \pm 3.3$, and $\alpha_4 = 2.9 \pm 3.8$). It could be interpreted that despite less availability of NO_3^- in passive areas, there is a more favorable environment for denitrification in passive regions of the wetland. This favorability for denitrification could be associated with less availability of oxygen in passive zones, as well as higher residence time in such areas.

Over the period of the research reported in this paper, $11{,}861.3 \pm 82.2$ kg of allochthonous organic carbon was washed into the wetland with inflow (Table 7). Of that amount, $2{,}508.5 \pm 518.7$ kg of OC (equivalent to $21.1 \pm 4.4\%$ of OC loading) was removed/retained through microbial decomposition, deposition of POC, and diffusion of DOC into wetland soil. The main removal process was microbial respiration (aerobic + anaerobic), which removed a total of 770.9 ± 584.6 kg of OC, equivalent to $6.5 \pm 4.9\%$ of the total inflow TOC load. Diffusion of DOC into the soil retained 286.5 ± 171.2 kg $(2.4 \pm 1.4\%)$, deposition of POC removed 242.1 ± 340.7 kg $(2.0 \pm 2.9\%)$ of TOC and 595.9 ± 36.8 kg of DOC ($5.0 \pm 0.3\%$ of OC loading) was lost to seepage (GW loss).

In general, the uncertainties associated with carbon processes were smaller than that of nitrogen cycling processes. The largest uncertainty belongs to mass of carbon lost to aerobic respiration, which has a SD of 322.7 kg, equivalent to 2.7% of TOC loading. However, TOC export had a slightly higher uncertainty compared to TN export (3.7 versus 2.3%).

Moving from the active to passive zones of the wetland (Compartments C.2–C.4), more deposition of OC occurred in active and transient zones (Compartments C.2 and C.3) compared to the passive zone (Compartment C.4). Similar to previous findings, the mass of all exchanges (physical and biogeochemical) decreased along the activity gradient. Another observed trend in the wetland is that anaerobic processes become more significant in moving along the activity gradient towards passive areas. The ratio of aerobic to anaerobic respiration declines continuously from Compartments C.2 to C.4 (2.14 ± 1.93 to 0.72 ± 0.94), indicating that the passive zone has more favorable conditions for denitrification and methanogenesis compared to the active zone. This finding is consistent to previous conclusions from the nitrogen mass balance analysis.

Summary and Conclusions

This paper presented the development and application of a compartmental wetland model that captures the full spectrum of biogeochemical interactions in active and passive zones of wetlands. This enhanced methodology upgraded model resolution in the horizontal domain by discretizing the spatial domain (wetland area) into compartments, and connecting neighboring compartments through advective and dispersive/diffusive exchange. The main goal of the research reported in this paper was to develop a model with acceptable performance, which has the ability to reflect the spatial variability of biogeochemical mass exchanges and concentrations throughout different zones of the wetland. A single compartment (lumped) model might perform equally well (or even outperform) compared to the compartmentalized model, but would lack the ability to provide the insight that the compartmentalized model is offering.

The compartmental model was applied to data collected from a restored wetland in California's Central Valley during the 2007 growing season. Due to the close proximity of inflow and outflow control structures different hydrologic environments were created within the study wetland, including the formation of a large stagnant zone. The wetland investigated in the research reported in this paper was divided into four compartments along the activity gradient from north to south (most active to most passive). Through a detailed sensitivity and mass balance analyses, it was aimed to identify the most important processes engaging nitrogen and carbon constituents along the activity gradient.

It was commonly observed that Compartment C.2 had the lowest posterior uncertainty among all compartments. Since observed data were collected from Compartment C.2, this compartment had the most influence on model fitness and the smallest uncertainty among all wetland compartments.

Mass balance analysis revealed that over the course of the period of the research reported in this paper, about $23.4 \pm 3.9\%$ of the incoming TN load and $21.1 \pm 4.4\%$ of the TOC load was removed or retained by SJRW. Moving from active to passive zones of the wetland (Compartments C.2–C.4), it was observed that the mass of all exchanges (physical and biogeochemical) regarding nitrogen and carbon cycling decreased along the activity gradient. More deposition of OC occurred in active and transient zones (Compartments C.2 and C.3) compared to the passive zone (Compartment C.4). It was also revealed that anaerobic processes become more significant along the activity gradient toward passive areas. Despite less availability of NO_3^- in passive areas, there was a more favorable environment for denitrification in passive regions of the wetland.

The K–S test based on model performance of TOC and TN export revealed that the most sensitive parameter for all compartments in the wetland is E_{fact} (magnification parameter for the processes of horizontal diffusion and dispersion between compartments). Parameter k_{dn}, representing the denitrification rate, was constantly an important parameter in active and passive zones, showing that denitrification is an important loss pathway for nitrogen in the entire wetland. Decomposition of DOC appeared to be the dominant carbon cycling process within the wetland, as parameters k_{1d}, k_{2d}, and k_{3d} appeared at the top of the sensitivity list for all compartments. The K–S test was not able to reveal information on important processes associated with carbon and nitrogen cycling that were specific to active or passive zones, likely due to the lack of data availability for all compartments of the wetland.

In the case study, the compartmentalized model made it possible to gain insight about deposition patterns of organic matter and showed that aerobic activity declines in the passive zones. However, the capabilities of the compartmentalized model were not exploited to their full extent, due to the lack of observed data for each wetland compartment.

High levels of nitrate and ammonium in the wetland may indicate that the SJRW wetland was reaching nitrogen saturation at the time of the research reported in this paper. Nitrogen saturation in wetlands severely impacts biogeochemical cycling of various nutrients. Indicators of a nitrogen saturated wetland include elevated rates of nitrification in soil, increased nitrate leaching to groundwater, increased nitrate concentrations in surface water outflows, acidification of soils, and aluminum mobilization to groundwater

(Hanson et al. 1994). The *WetQual* model does not directly consider effects of nitrogen saturation on biogeochemistry of wetlands. Addition of a related relationship to address such effects may enhance model performance in wetlands similar to SJRW which receive agricultural tailwater with elevated nitrogen levels.

The monitoring period for this case study was limited to 4 months during the active growing season of 2007. A much longer monitoring period would have been beneficial for the research reported in this paper. The short monitoring period in this case study symbolizes a larger problem in the field of wetland modeling where acquiring good quality field monitoring data is generally a big obstacle. In addition, when field data exists, it is common that not all the components within a specific elemental cycle are monitored. For instance, in the case of this study, gaseous end-products of nitrogen and carbon cycles (methane, carbon dioxide, and nitrous oxide) were not monitored. This prevented validation of the methane component in the *WetQual* model, and ultimately introduced uncertainty in judgments made on the basis of mass balance analysis.

Acknowledgments

The U.S. EPA through its Office of Research and Development partially funded and collaborated in the research reported in this paper under Contract EP-C-11-006 with Auburn University, School of Forestry and Wildlife Sciences. It has not been subject to the EPA review and therefore does not necessarily reflect the views of the EPA, and no official endorsement should be inferred.

References

Akaike, H. (1974). "A new look at the statistical model identification." *IEEE Trans. Autom. Control*, 19(6), 716–723.

Anderson, C. J., and Mitsch, W. J. (2006). "Sediment, carbon, and nutrient accumulation at two 10-year-old created riverine marshes." *Wetlands*, 26(3), 779–792.

Beven, K., and Binley, A. (1992). "The future of distributed models: Model calibration and uncertainty prediction." *Hydrol. Process.*, 6(3), 279–298.

Carnahan, B., Luther, H. A., and Wilkes, J. O. (1969). *Applied numerical methods*, Wiley, New York.

Cerco, C. F., and Cole, T. (1995). *User's guide to the CE-QUAL-ICM three-dimensional eutrophication model: Release version 1.0*, Waterways Experiment Station, U. S. Army Corps of Engineers, Vicksburg, MS.

Chapra, S. C. (1997). *Surface water-quality modeling*, McGraw–Hill, New York.

CIMIS (California Irrigation Management Information System). (2007). "*Climate*." ⟨http://wwwcimis.water.ca.gov/cimis/welcome.jsp⟩ (Feb. 17, 2015).

Cohn, T. A., Caulder, D. L., Gilroy, E. J., Zynjuk, L. D., and Summers, R. M. (1992). "The validity of a simple statistical model for estimating fluvial constituent loads: An empirical study involving nutrient loads entering Chesapeake Bay." *Water Resour. Res.*, 28(9), 2353–2363.

DHI (Danish Hydraulic Institute). (2004). *Coastal hydraulics and oceanography user guide*, Hørsholm, Denmark.

Di Toro, D. M. (2001). *Sediment flux modeling*, Wiley, New York.

Dunne, T. (1978). *Water in environmental planning*, Macmillan, New York.

Fischer, H. B. (1979). *Mixing in inland and coastal waters*, Elsevier, Amsterdam, Netherlands.

Haan, C. T. (2002). *Statistical methods in hydrology*, Iowa State University Press, Ames, IA.

Hanson, G. C., Groffman, P. M., and Gold, A. J. (1994). "Symptoms of nitrogen saturation in a riparian wetland." *Ecol. Appl.*, 4(4), 750–756.

Hantush, M., Kalin, L., Isik, S., and Yucekaya, A. (2013). "Nutrient dynamics in flooded wetlands: I. Model development." *J. Hydrol. Eng.*, 10.1061/(ASCE)HE.1943-5584.0000741, 1709–1723.

Ji, Z.-G. (2008). *Hydrodynamics and water quality: Modeling rivers, lakes, and estuaries*, Wiley, Hoboken, NJ.

Jørgensen, S. E., and Bendoricchio, G. (2001). *Fundamentals of ecological modelling*, Elsevier, Amsterdam, Netherlands.

Kadlec, R. H., and Hammer, D. E. (1988). "Modeling nutrient behavior in wetlands." *Ecol. Modell.*, 40(1), 37–66.

Kadlec, R. H., and Wallace, S. (2008). *Treatment wetlands*, CRC, Boca Raton, FL.

Kalin, L., Hantush, M., Isik, S., Yucekaya, A., and Jordan, T. (2013). "Nutrient Dynamics in flooded wetlands. II: Model application." *J. Hydrol. Eng.*, 10.1061/(ASCE)HE.1943-5584.0000750, 1724–1738.

Kutner, M. H., Nachtsheim, C. J., Neter, J., and Li, W. (2005). *Applied linear statistical models*, McGraw–Hill, New York.

Liang, X., et al. (2007). "Modeling transport and fate of nitrogen from urea applied to a near-trench paddy field." *Environ. Pollut.*, 150(3), 313–320.

Little, K. W. (2012). *Environmental fate and transport analysis with compartment modeling*, CRC, Boca Raton, FL.

Massey, F. J., Jr. (1951). "The Kolmogorov–Smirnov test for goodness of fit." *J. Am. Stat. Assoc.*, 46(253), 68–78.

Maynard, J. (2009). "Biogeochemical cycling and retention of carbon and nutrients in a constructed wetland receiving agricultural runoff in the San Joaquin Valley, California." Ph.D. thesis, Univ. of California, Davis, CA.

Maynard, J. J., O'Geen, A. T., and Dahlgren, R. A. (2011). "Sulfide induced mobilization of wetland phosphorus depends strongly on redox and iron geochemistry." *Soil Sci. Soc. Am. J.*, 75(5), 1986–1999.

Min, J. H., and Wise, W. R. (2009). "Simulating short-circuiting flow in a constructed wetland: The implications of bathymetry and vegetation effects." *Hydrol. Process.*, 23(6), 830–841.

Mitsch, W. J., and Gosselink, J. G. (2007). *Wetlands*, Wiley, Hoboken, NJ.

Penman, H. L. (1948). "Natural evaporation from open water, bare soil and grass." *Proc. Roy. Soc. London Ser. A Math. Phys. Sci.*, 193(1032), 120–145.

Pivato, A., and Raga, R. (2006). "Tests for the evaluation of ammonium attenuation in MSW landfill leachate by adsorption into bentonite in a landfill liner." *Waste Manage.*, 26(2), 123–132.

Reddy, K. R., and DeLaune, R. D. (2008). *Biogeochemistry of wetlands: Science and applications*, CRC, Boca Raton, FL.

Runkel, R. L., Crawford, C. G., and Cohn, T. A. (2004). *Load estimator (LOADEST): A FORTRAN program for estimating constituent loads in streams and rivers*, USGS, Reston, VA.

Schnoor, J. L. (1996). *Environmental modeling: Fate and transport of pollutants in water, air, and soil*, Wiley, Hoboken, NJ.

Sharifi, A., Kalin, L., Hantush, M. M., Isik, S., and Jordan, T. E. (2013). "Carbon dynamics and export from flooded wetlands: A modeling approach." *Ecol. Modell.*, 263, 196–210.

Spear, R., and Hornberger, G. (1980). "Eutrophication in peel inlet—II. Identification of critical uncertainties via generalized sensitivity analysis." *Water Res.*, 14(1), 43–49.